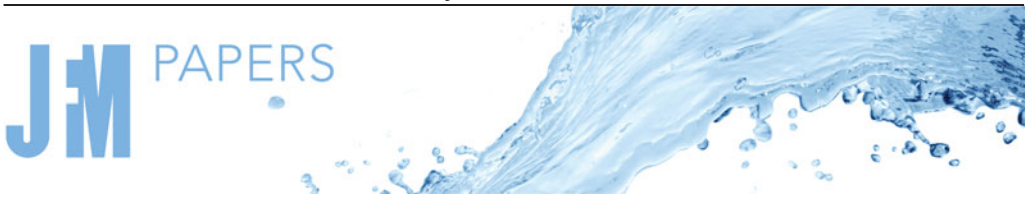
CrossMark

J. Fluid Mech. (2021), *vol*. 920, A2, doi:10.1017/jfm.2021.308



Non-continuum tangential lubrication gas flow between two spheres

Melanie Li Sing How[1], Donald L. Koch[2] and Lance R. Collins[1,3,†]

[1]Sibley School of Mechanical and Aerospace Engineering, Cornell University, Ithaca, NY 14853, USA

[2]Smith School of Chemical and Biomolecular Engineering, Cornell University, Ithaca, NY 14853, USA

[3]Innovation Campus, Virginia Tech, 3000 Potomac Avenue, Suite 101 Alexandria, VA 22305, USA

(Received 13 December 2020; revised 4 March 2021; accepted 30 March 2021)

As two particles approach each other, the continuum lubrication force diverges, with decreasing separation preventing contact. However, for separations comparable to the mean free path of the gas, λ, non-continuum effects cause the lubrication force to diverge more slowly with decreasing separation distance, allowing for contact in finite time. The first study of this phenomenon was done by Sundararajakumar & Koch (*J. Fluid Mech.*, vol. 313, 1996, pp. 238–308) for two particles moving along their line of centres. We extend their normal motion study to include tangential motions. For small Knudsen number $Kn = \lambda/a$, where a is the harmonic mean of the two particle radii, we use a matched asymptotic expansion technique to obtain the non-continuum forces and torques for tangential motions of spheres separated by distances within the lubrication regime that are at or below the mean free path of the gas. The hydrodynamic resistivity functions are fitted to provide a uniformly valid approximation that smoothly transitions between the continuum multipole and non-continuum lubrication expressions for the forces and torques as the minimum gap between the particles h_0 varies from values of $O(a)$ to values of $O(\lambda)$. These functions, in combination with the result by Sundararajakumar & Koch (*J. Fluid Mech.*, vol. 313, 1996, pp. 238–308) and the classical work by Jeffrey & Onishi (*J. Fluid Mech.*, vol. 139, 1984, pp. 261–290), yield a complete formulation for the hydrodynamic interactions of two spheres at all separations, from non-interacting spheres in the extreme far field through all the transitions that occur up to contact. We apply the new formulation to the classical case of a particle settling parallel to a vertical wall. The continuum Stokes equation predicts a settling speed that decreases with decreasing gap separation and vanishes at contact, whereas the non-continuum model developed herein predicts a finite settling speed at contact.

Key words: drops, lubrication theory

† Email address for correspondence: lc246@cornell.edu

© The Author(s), 2021. Published by Cambridge University Press

https://doi.org/10.1017/jfm.2021.308 Published online by Cambridge University Press

1. Introduction

The hydrodynamic interaction between particles moving relative to each other is important in many applications involving sedimentation and suspensions of small particles, such as pneumatic transport and fluidized beds (Klinzing 2001). In atmospheric clouds, droplets with diameters greater than 30 μm grow predominantly by coalescence driven by gravitational settling and atmospheric turbulence (Shaw 2003). For diameters smaller than 100 μm, surface deformation can be neglected (Devenish *et al.* 2012). Interfacial mobility is negligible due to the high ratio of viscosity of the drop and gas (Davis, Schonberg & Rallison 1989). Furthermore, the flow in the gap between the droplets is nearly incompressible with negligible gas inertia because of the low Mach and Reynolds numbers. Quantitative estimates of the aforementioned effects for drops interacting by differential sedimentation are given in figure 2 of Dhanasekaran, Roy & Koch (2021). According to the Stokes equation, the resistance experienced by two approaching droplets diverges with decreasing separation, preventing contact (Happel & Brenner 1983). In the absence of some mitigating factor, cloud droplets could only grow by condensation. In the size range where coalescence becomes important, the hydrodynamic force generated by the lubrication flow diverges more slowly than that predicted by the Stokes equation at separations below the mean free path of the gas. This weaker divergence of the force, due to non-continuum effects of the gas, allows coalescence to occur in finite time.

We consider the classical problem of two distinct, hydrodynamically interacting spheres. Hydrodynamic interaction (HI) refers to the forces and torques that one sphere exerts upon the other through the fluid. There are two complementary frameworks for HI. When the forces and torques are expressed in terms of a given set of velocities, Brenner & O'Neill (1972) defined the problem as a 'resistivity' problem, whereas the converse of expressing the velocities as functions of the forces and torques was termed the 'mobility' problem by Batchelor (1982). The velocities and rotation rates of particles with negligible inertia can be determined in terms of the forces and torques using a mobility formulation. However, for inertial particles, the case of interest here, the translational and rotational velocities are dynamic variables and the forces and torques must be determined from them using a resistivity formulation.

The resistivity (or mobility) matrix is made up of 16 3×3 tensors. Jeffrey & Onishi (1984) showed that an arbitrary motion of two spheres in a fluid can be expressed as a linear combination of four independent motions involving six resistivities:

(i) force $f_t^{\parallel}$ due to translation parallel to their line of centres;
(ii) torque $t_r^{\parallel}$ due to rotation on the axis parallel to their line of centres;
(iii) force $f_t^{\perp}$ and torque $t_t^{\perp}$ due to translation perpendicular to their line of centres; and
(iv) force $f_r^{\perp}$ and torque $t_r^{\perp}$ due to rotation on an axis perpendicular to their line of centres;

where the subscripts 't' and 'r' refer to translation and rotation, respectively, and the superscripts $\parallel$ and $\perp$ represent the directions parallel and perpendicular to their line of centres, respectively. This study addresses the resistivity functions associated with all tangential motions described in (iii) and (iv).

As noted above, we are interested in the relative motion of spheres with mean radius, a, of the order of tens to hundreds of microns. This is an important size range in atmospheric clouds, as the dominant mechanism for growth switches from condensation to coalescence. Defining the minimum gap separation, h_0, as the distance between two sphere surfaces along their line of centres and a as the harmonic mean radius, for $\varepsilon \equiv h_0/a \geq O(1)$, the

https://doi.org/10.1017/jfm.2021.308 Published online by Cambridge University Press

Stokes flow solution can be expressed as a twin multipole expansion, as described by Jeffrey & Onishi (1984).

In the limit $\varepsilon \ll 1$, the spheres can be thought of as 'near contact'. The flow between the spheres is best described by lubrication theory, which gives the leading-order solution in the asymptotic expansion of the small parameter, ε. As ε decreases, the continuum lubrication solution dominates the resistivities causing the normal resistivity, $f_t^{\parallel}$, to diverge like ε^{-1} and the tangential resistivities, $f_t^{\perp}$, $f_r^{\perp}$, $t_t^{\perp}$ and $t_r^{\perp}$ to diverge like $\ln(\varepsilon^{-1})$. The important physical result of these divergences is that two spheres on a colliding trajectory could never touch (coalesce). Likewise, a sphere in contact with a vertical wall in gravity would remain stationary owing to the diverging tangential force. Both results are inconsistent with observations, suggesting the continuum approximation is no longer an adequate description.

The mean free path of air at atmospheric pressure is $\lambda \approx 70$ nm. At gap separations of the order of the mean free path of the gas the continuum approximation breaks down. Hocking & Jonas (1970) simply chose an arbitrary gap distance to allow for the coalescence of two particles, while Hocking (1973) extended the analysis further by solving the lubrication flow between the spheres using the Maxwell slip boundary condition. This is a reasonable approximation when h_0/λ is large but finite and non-continuum effects are confined to thin regions near the sphere surfaces. However, it breaks down in the 'transition regime' when $h_0/\lambda = O(1)$ and the frequency of molecular–wall collisions is comparable with that of intermolecular collisions.

The non-continuum flow is governed by the Boltzmann equation, which is a nonlinear integro-differential equation that is computationally expensive to solve, even with modern computers. At the small Mach numbers characteristic of typical μm-scale particle motions in a gas, the Boltzmann equation can be linearized. A further simplification is afforded if the intermolecular collisions are replaced by a collision operator that relaxes the molecular velocity toward a Maxwellian distribution relative to the local mean gas velocity, leading to the Bhatnagar–Gross–Krook (BGK) approximation to the linearized Boltzmann equation (Bhatnagar, Gross & Krook 1954). Cercignani & Pagani (1966) solved the BGK model for the flux and the stresses of Poiseuille and Couette flows between two flat plates. Sundararajakumar & Koch (1996) used those results, incorporating surface curvature and employing the incompressible mass conservation equation, to obtain a modified resistivity for the normal motion of two spheres all the way up to contact. Additionally, they corrected the small error in the mean free path resulting from the assumption of a Maxwellian velocity distribution, and curve fit the results to obtain a resistivity over the full range of separations from free molecular to continuum lubrication flow. In particular, they showed that in the case of squeezing flow, the force $f_t^{\parallel}$ in the free molecular regime diverges more weakly as $\ln[\ln(\varepsilon^{-1})]$, thus allowing particles to come into contact in finite time. Gopinath, Chen & Koch (1997) studied the effects of compressibility on non-continuum lubrication squeezing flows that arise when the characteristic lubrication pressure becomes as large as the atmospheric pressure when $h_0 = O(\lambda)$. Compressibility effects are small for particles with radii less than 50 μm colliding at velocities comparable with their terminal velocities, and they will be neglected in the present study. Likewise, we apply the quasi-steady approximation under the assumption that the flow time scale (gap divided by the relative velocity) is much larger than the molecular collision time (mean free path divided by the speed of sound), which is valid for small Mach numbers.

This study extends the work of Sundararajakumar & Koch (1996) to obtain expressions for the four tangential resistivity functions. The problem set-up, geometry and scaling are described in § 2. Section 3 presents the non-continuum flow analysis and the results

https://doi.org/10.1017/jfm.2021.308 Published online by Cambridge University Press

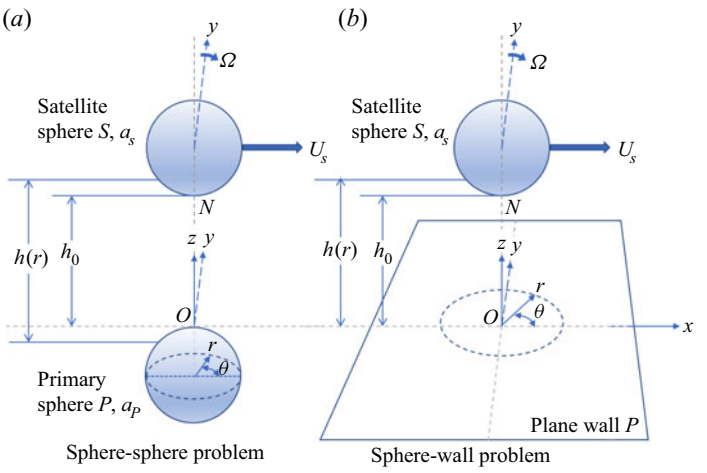


Figure 1. Sketch in isometric view of the sphere S in cylindrical coordinates with the minimum gap separation h_0 measured from the nearest point N on S to the origin O on sphere P (a) and on plane P (b).

for the uniformly valid resistivity functions for tangential translation and rotation. This includes a convenient curve fit that provides a single relationship that applies across all regimes. The relationship between the present non-continuum analysis and Hocking (1973), who introduced the Maxwell slip boundary conditions to account for the first effect of the non-continuum gas, is given in § 3.4. Section 4 applies the uniformly valid resistivity functions to the classical problem of a sphere settling adjacent to a vertical wall, highlighting the important effects of the non-continuum gas flow between the particle and the wall when $h_0/\lambda < 1$. Conclusions are presented in § 5.

2. Problem statement

Figure 1 shows a sketch of the two spheres. We designate sphere 'P' as the 'primary' sphere and sphere 'S' as the 'satellite' sphere. We consider the fluid motion generated by the translation and rotation of sphere S relative to sphere P at rest at the origin. The fluid is an infinite gas with a density ρ and viscosity μ. Defining the radii of the primary and satellite spheres as a_P and a_S, respectively, the harmonic mean radius is

$$a = \frac{a_S a_P}{a_S + a_P}. \tag{2.1}$$

As we are concerned with tangential HI, we consider sphere S moving with translational velocity of $(U_S, 0, 0)$ and angular velocity of $(0, a_S\Omega, 0)$ in Cartesian coordinates.

We assume the Reynolds and Mach numbers of the flow are vanishingly small allowing us to neglect fluid inertia and use results obtained from the linearized Boltzmann equation, treating incompressibility as discussed in Gopinath *et al.* (1997). As we are concerned with non-continuum effects at small separations, we introduce the Knudsen number defined as $Kn \equiv \lambda/a$, where recall λ is the mean free path of the gas. The analysis will be restricted to the large sphere limit, $Kn \ll 1$. The non-dimensional parameter characterizing the separation of the spheres is defined as $\varepsilon \equiv h_0/a$, where h_0 is the minimum separation distance of the sphere surfaces (see figure 1). In terms of the non-continuum analysis, the relevant non-dimensional separation is given by $\delta_0 \equiv h_0/\lambda$. Note that, by definition, $\varepsilon = \delta_0 Kn$, which implies $\varepsilon \ll \delta_0$.

https://doi.org/10.1017/jfm.2021.308 Published online by Cambridge University Press

2.1. *Spheres widely separated*

For $\delta_0 \gg 1$, the governing equations for the fluid are the Stokes equation and continuity

$$\boldsymbol{\nabla} p = \mu \nabla^2 \boldsymbol{u}, \quad \boldsymbol{\nabla} \cdot \boldsymbol{u} = 0, \tag{2.2a,b}$$

where $\boldsymbol{u}$ is the fluid velocity and p is the pressure.

Figure 1 shows the cylindrical coordinate system that will be used to analyse the flow in the gap. In cylindrical coordinates (r, θ, z), the dimensional gap separation $h(r)$ with minimum gap separation h_0 is given by

$$h(r) = h_0 + \left(a_S - \sqrt{a_S^2 - r^2}\right) + \left(a_P - \sqrt{a_P^2 - r^2}\right). \tag{2.3}$$

For $\varepsilon \geq O(1)$, the disturbance velocity field of a sphere can be written as a multipole expansion about its centre (Kim & Karrila 1991). The leading-order terms for the far field can be calculated by the method of reflections, but this becomes computationally expensive, as the number of terms required for a given accuracy increases with decreasing separation. Jeffrey & Onishi (1984) developed the twin multipole expansion method that expresses Lamb's solution expanded with respect to two different origins. The result is a tractable means for computing the HIs of two spheres of arbitrary size ratio down to separations as small as $\varepsilon \gtrsim 0.1$.

2.2. *Spheres in near contact*

In the limit $\varepsilon \ll 1$ and $\delta_0 \gg 1$, the continuum flow in the gap obeys the Stokes equation and can be analysed using a matched asymptotic analysis. O'Neill & Stewartson (1967) identified an 'inner region', where they applied the standard lubrication approximation, and an 'outer region', where the full Stokes equations were used. The solutions are equated at a radial distance r_M. Figure 2 depicts the 'inner' and 'outer' regions. In the inner region, we are interested in the limit $r \ll a_P$ and $r \ll a_S$, allowing us to introduce a Taylor series expansion for the two square roots in (2.3), yielding

$$h(r) = h_0 + a_S\left[1 - \left(1 - \frac{1}{2a_S^2}r^2 - \frac{1}{8a_S^4}r^4 \ldots\right)\right] + a_P\left[1 - \left(1 - \frac{1}{2a_P^2}r^2 - \frac{1}{8a_P^4}r^4 \ldots\right)\right]. \tag{2.4}$$

Rearranging (2.4) and introducing (2.1) yields

$$\frac{h(r)}{h_0} = 1 + \frac{1}{2}\left(\frac{1}{ah_0}\right)r^2 + \frac{1}{8}\left(\frac{1}{ah_0}\right)^2 r^4 \ldots. \tag{2.5}$$

The independent variables are made dimensionless as

$$R \equiv \frac{r}{\sqrt{ah_0}}, \quad Z \equiv \frac{z}{h_0}. \tag{2.6a,b}$$

To leading order, the dimensionless gap of (2.5) is expressed as

$$H(R) \equiv \frac{h(r)}{h_0} = 1 + \frac{1}{2}R^2. \tag{2.7}$$

The equations defining the surfaces of the two spheres are then defined as

$$\left.\begin{aligned} Z_S &= 1 + \tfrac{1}{2}\alpha R^2, \\ Z_P &= -\tfrac{1}{2}(1-\alpha)R^2, \end{aligned}\right\} \tag{2.8}$$

https://doi.org/10.1017/jfm.2021.308 Published online by Cambridge University Press

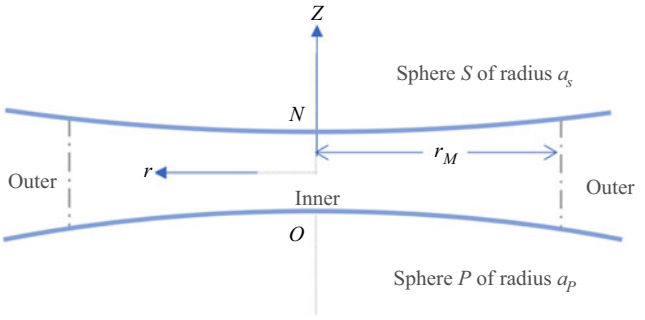


Figure 2. Sketch of the inner region defined as $0 < r < r_M$ and outer region defined as $r > r_M$.

where α is the size ratio

$$\alpha \equiv \frac{a}{a_S}, \tag{2.9}$$

and consequently $\alpha \to 1$ for $a_P/a_S \to \infty$ and $\alpha \to 0$ for $a_S/a_P \to \infty$.

The velocity components and pressure can be written as (O'Neill & Stewartson 1967)

$$\left.\begin{aligned} u_r(r,\theta,z) &= U_S\, U(R,Z)\cos\theta, \\ u_\theta(r,\theta,z) &= U_S\, V(R,Z)\sin\theta, \\ u_z(r,\theta,z) &= U_S\, W(R,Z)\cos\theta, \\ p(r,\theta,z) &= \frac{\mu U_S}{a} P(R,Z)\cos\theta, \end{aligned}\right\} \tag{2.10}$$

where U, V and W are the dimensionless velocity components and P is the dimensionless pressure. The resulting dimensionless governing equations become

$$\left.\begin{aligned} \varepsilon^{3/2}\frac{\partial P}{\partial R} &= -\varepsilon\left[\frac{2(U+V)}{R^2} + \frac{\partial^2 U}{\partial R^2}\right] + \frac{\partial^2 U}{\partial Z^2}, \\ -\varepsilon^{3/2}\frac{P}{R} &= -\varepsilon\frac{2(U+V)}{R^2} + \frac{\partial^2 V}{\partial Z^2}, \\ \varepsilon^{3/2}\frac{\partial P}{\partial Z} &= \varepsilon^{3/2}\left[\frac{\partial^2 W}{\partial R^2} + \frac{1}{R}\frac{\partial W}{\partial R} - \frac{W}{R^2}\right] + \varepsilon^{1/2}\frac{\partial^2 W}{\partial Z^2} \end{aligned}\right\} \tag{2.11}$$

and the continuity equation is

$$\frac{\partial U}{\partial R} + \frac{U+V}{R} + \frac{1}{\varepsilon^{1/2}}\frac{\partial W}{\partial Z} = 0. \tag{2.12}$$

Equation (2.12) implies that both U and V are $O(1)$ and W is order $\varepsilon^{1/2}$. It follows from (2.11) that the pressure, P, scales as $\varepsilon^{-3/2}$. A regular expansion in ε is then assumed to take the form

$$\left.\begin{aligned} U(R,Z) &= U_0(R,Z) + \varepsilon U_1(R,Z) + \ldots, \\ V(R,Z) &= V_0(R,Z) + \varepsilon V_1(R,Z) + \ldots, \\ W(R,Z) &= \varepsilon^{1/2} W_0(R,Z) + \varepsilon^{3/2} W_1(R,Z) + \ldots, \\ P(R,Z) &= \varepsilon^{-3/2} P_0(R,Z) + \varepsilon^{-1/2} P_1(R,Z) + \ldots. \end{aligned}\right\} \tag{2.13}$$

https://doi.org/10.1017/jfm.2021.308 Published online by Cambridge University Press

To leading order, the governing equations (2.11) and (2.12) become

$$\frac{\partial P_0}{\partial R} = \frac{\partial^2 U_0}{\partial Z^2}, \quad -\frac{P_0}{R} = \frac{\partial^2 V_0}{\partial Z^2}, \quad \frac{\partial P_0}{\partial Z} = 0, \tag{2.14a–c}$$

$$\frac{\partial U_0}{\partial R} + \frac{U_0 + V_0}{R} + \frac{\partial W_0}{\partial Z} = 0. \tag{2.15}$$

3. Non-continuum flow analysis

For separation distances below the mean free path, i.e. $\delta_0 \leq O(1)$, non-continuum effects become important and the Stokes equation (cf. 2.2*a*,*b*) is no longer a valid representation of the inner flow. The continuity equation continues to hold for a non-continuum gas whose pressure variation is small compared to the ambient pressure, as do the ε scalings in (2.10), except the variables are functions of δ_0 too. To analyse the non-continuum velocity and pressure, we replaced the Stokes equation for the inner region of the lubrication layer with the BGK approximation to the linearized Boltzmann equation (Bhatnagar *et al.* 1954). As shown in § 3.1, we employ BGK solutions for Poiseuille and Couette flows from the literature to construct the inner solution for the lubrication layer. Note that, because we assume $Kn \ll 1$, the outer flow is in the continuum regime even when the inner flow is not (all the way up to contact), simplifying the matching process.

3.1. *Decomposition of the lubrication flow*

Under the standard lubrication approximation, the local flow between the two spheres can be represented as a superposition of Poiseuille, Couette and plug flows, as depicted in figure 3. Poiseuille flow is characterized by the pressure gradient driving the flow, whereas Couette flow is characterized by the shear rate between the two surfaces. Plug flow assumes a uniform velocity across the channel. Its role is to allow arbitrary boundary conditions to be satisfied. Poiseuille and plug flows contribute to the mass flux through the gap while Poiseuille and Couette flows contribute to the shear stress on the sphere surfaces. The weights associated with the Couette and plug flows are determined by the boundary conditions.

Recall this study is concerned with the forces and torques associated with tangential motions of the spheres. In the Cartesian coordinate system shown in figure 1, the tangential motion between the spheres arises from a combination of translation of sphere S in a direction perpendicular to the line of centres, given by $(U_S, 0, 0)$, and its rotation along an axis perpendicular to the line of centres, defined as $(0, \Omega a_S, 0)$. The resulting x velocity of the surface of sphere S, U_{wall} (see figure 3), can be approximated in the inner region as

$$U_{wall} = U_S(1 - \omega), \tag{3.1}$$

where

$$\omega = \frac{\Omega a_S}{U_S}. \tag{3.2}$$

Below, we show how the boundary conditions are used to obtain the weighting of Couette and plug flows. However, first we must account for the non-continuum Poiseuille and Couette flows in the gap.

3.1.1. *Poiseuille flow*

Cercignani & Daneri (1963) analysed the pressure-driven flow of a rarefied gas between two parallel plates using the BGK model (Bhatnagar *et al.* 1954). For consistency with the

https://doi.org/10.1017/jfm.2021.308 Published online by Cambridge University Press

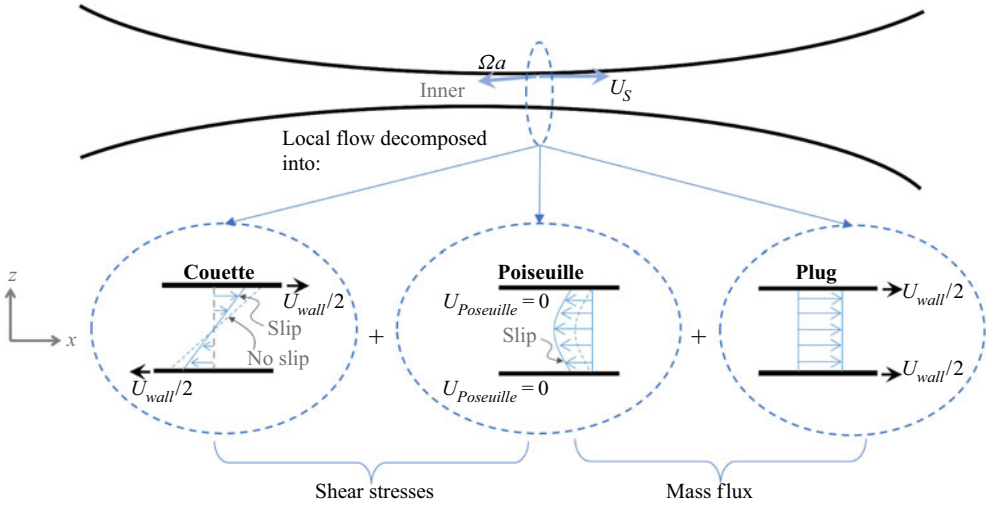


Figure 3. Sketch of the inner region in the xz plane decomposed into three planar flows: Couette, Poiseuille and plug flows. The Poiseuille flow depends upon the pressure gradient, the mass flux is determined by the plug and Poiseuille flows, and the shear stresses are obtained from the Poiseuille and Couette flows.

analysis for spheres given below, we designate the separation distance between the plates h and the dimensionless separation, $\delta = h/\lambda$. The volumetric flux, defined as the average velocity integrated across the channel, is proportional to the average pressure gradient in all regimes, i.e. the pseudo-free molecular regime ($\delta \ll 1$), transition ($\delta = O(1)$) and continuum regime ($\delta \gg 1$). The general dimensionless expression is given by

$$\int_0^1 U(Z)\,\mathrm{d}Z = -\frac{g(\delta)}{2\delta}\frac{\mathrm{d}P}{\mathrm{d}X}, \tag{3.3}$$

where we apply the same scaling as described in § 2.2 and $g(\delta)$ is a dimensionless function that accounts for the transitions through the different regimes. The limit $\delta \ll 1$ corresponds to the pseudo-free molecular regime, where $g(\delta)$ has an analytical form. Likewise in the limit $\delta \gg 1$, the solution approaches the Hagen Poiseuille law with a slip coefficient, $k_1 = 1.016$ (see § 3.4 for a definition and more complete explanation of the slip coefficient). In the transition regime, the values were numerically evaluated and tabulated by Cercignani & Daneri (1963). The resulting expression for $g(\delta)$ is

$$g(\delta) = \begin{cases} -\dfrac{1}{\sqrt{\pi}}(-\ln\delta + 0.8), & (\delta < 0.01), \\ V(\delta), & (0.01 < \delta < 10), \\ \dfrac{\delta}{6} + k_1, & (\delta > 10), \end{cases} \tag{3.4}$$

where $\delta < 0.01$ corresponds to the pseudo-free molecular regime, $\delta > 10$ corresponds to the continuum flow regime and $V(\delta)$ represents a curve fit of the tabulated results from Cercignani & Daneri (1963). Figure 4 shows a plot of $g(\delta)$. The markers (•) are the tabulated values, the solid line is the cubic spline fit, and the limiting solutions for the pseudo-free molecular and continuum regimes are the dashed and dash-dot lines, respectively.

https://doi.org/10.1017/jfm.2021.308 Published online by Cambridge University Press

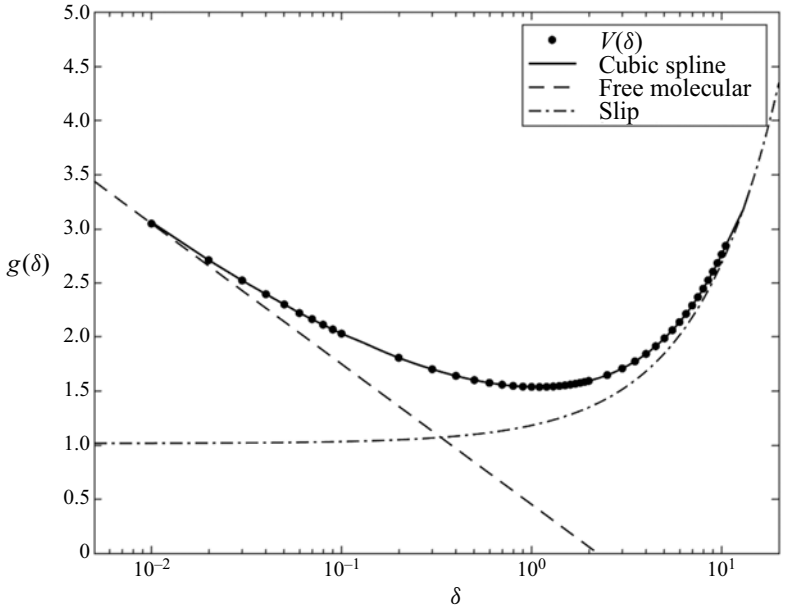


Figure 4. The $g(\delta)$ function (3.4) showing the tabulated results of Cercignani & Daneri (1963) (•), the cubic spline fit used to interpolate between the points (line) and the limiting solutions for the pseudo-free molecular (dashed line) and slip (dash-dot line) regimes.

3.1.2. *Couette flow*

In the case of planar Couette flow, the variable of interest is the shear stress in terms of the velocity difference between the top and bottom walls. Linearity and symmetry imply that the normal stress differences in low-Mach-number non-continuum planar Couette flow are zero, just as they are for low-Reynolds-number continuum Couette flow. We consider the motion of a rarefied gas between two parallel plates separated by a distance, h, with the top plate moving with a velocity $U_{wall}/2$ and the bottom plate moving with a velocity $-U_{wall}/2$, creating a velocity difference across the channel of U_{wall}. In the free molecular limit (i.e. $\delta = h/\lambda \to 0$), the linearized Boltzmann equation can be solved analytically for small Mach number (Kogan 1969). The velocity of the rarefied gas in this limit is constant over the gap and equal to the arithmetic mean of the wall velocities such that the dimensional free molecular shear stress τ_{xz}^{fm} in the xz plane is given by

$$\tau_{xz}^{fm} = -\frac{\mu U_{wall}}{\sqrt{\pi}\lambda}, \tag{3.5}$$

where $\mu = (1/2)\rho c\lambda$ is the molecular viscosity, $c = \sqrt{2p/\rho}$ is the mean molecular speed, ρ is the density and p is the thermodynamic pressure. Sharipov (2016) used the method of successive approximations based on the linearized Boltzmann equation to obtain the first order correction to the stress for small values of δ. If we non-dimensionalize the stress with the free molecular stress in (3.5), the resulting expression is

$$\frac{\tau_{xz}}{\tau_{xz}^{fm}} = 1 - \frac{\sqrt{\pi}}{2}\delta. \tag{3.6}$$

https://doi.org/10.1017/jfm.2021.308 Published online by Cambridge University Press

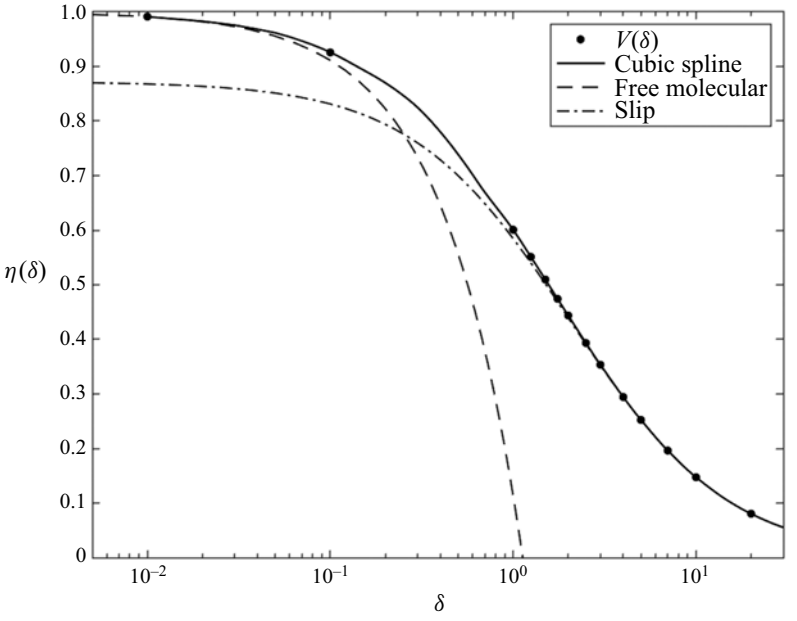


Figure 5. The $\eta(\delta)$ function (3.9) showing the tabulated results of Cercignani & Pagani (1966) (•), the cubic spline fit used to interpolate between the points (line) and the limiting solutions for the free molecular (dashed line) and slip (dash-dot line) regimes.

In the continuum limit (i.e. $\delta \gg 1$), the solution approaches the Couette solution with slip boundary conditions

$$\frac{\tau_{xz}}{\tau_{xz}^{fm}} = \frac{\sqrt{\pi}}{\delta + 2k_1}, \tag{3.7}$$

where once again k_1 is the slip coefficient.

In the transition region, Cercignani & Pagani (1966) solved the linearized Boltzmann equation using a variational principle with cutoff points approaching the limits. We can define a comprehensive expression for the stress across all regimes by introducing the dimensionless function $\eta(\delta)$, defined as

$$\eta(\delta) = \frac{\tau_{xz}}{\tau_{xz}^{fm}}, \tag{3.8}$$

which takes the form

$$\eta(\delta) = \begin{cases} 1 - \dfrac{\sqrt{\pi}}{2}\delta, & (\delta < 0.1), \\ Y(\delta), & (0.1 < \delta < 10), \\ \dfrac{\sqrt{\pi}}{\delta + 2k_1}, & (\delta > 10), \end{cases} \tag{3.9}$$

where $Y(\delta)$ is a cubic spline fit of the tabulated values obtained by Cercignani & Pagani (1966). The plot of $\eta(\delta)$ as a function of δ is shown in figure 5. The markers (•) are the tabulated values, the solid line is the cubic spline fit, and the limiting solutions for the free molecular and continuum regimes are the dashed and dash-dot lines, respectively.

https://doi.org/10.1017/jfm.2021.308 Published online by Cambridge University Press

Lastly, we note that there are no non-continuum effects to plug flow. So the above solutions for Poiseuille and Couette flows are all that we need to define the inner solution to the lubrication analysis. The next section discusses how the pressure field in the gap between the spheres is determined.

3.2. *Inner pressure field*

Sundararajakumar & Koch (1996) extended the results of Cercignani & Daneri (1963) to include the effects of curvature so that the analysis could be applied to the inner region of the lubrication flow between the spheres. The approach taken here is identical except now applied to the translation of sphere S in the x-direction and rotation along the y-axis, i.e. perpendicular to the line of centres. The flow in the gap is represented locally as a superposition of Couette, Poiseuille and plug flows. However, because of curvature, the resulting velocity is two-dimensional. Integrating the continuity equation (2.15) across the gap yields

$$\int_{Z_P}^{Z_S} \frac{\partial U_0}{\partial R}\,\mathrm{d}Z + \frac{1}{R}\int_{Z_P}^{Z_S} (U_0 + V_0)\,\mathrm{d}Z + \int_{Z_P}^{Z_S} \frac{\partial W_0}{\partial Z}\,\mathrm{d}Z = 0. \tag{3.10}$$

The final term can be evaluated in terms of the kinematic boundary condition at the two sphere surfaces, which can be written as

$$W_0(R, Z_P) = 0, \quad W_0(R, Z_S) = [(U_0(R, Z_S) - 1)]\alpha R. \tag{3.11a,b}$$

We rewrite the first term in (3.10) using Leibniz's rule

$$\int_{Z_P}^{Z_S} \frac{\partial U_0}{\partial R}\,\mathrm{d}Z = \frac{\mathrm{d}}{\mathrm{d}R}\left(\int_{Z_P}^{Z_S} U_0\,\mathrm{d}Z\right) - U_0(R, Z_S)\frac{\mathrm{d}Z_S}{\mathrm{d}R} + U_0(R, Z_P)\frac{\mathrm{d}Z_P}{\mathrm{d}R}. \tag{3.12}$$

Introducing the variable change

$$\tilde{x} = \tfrac{1}{2}R^2 \quad \rightarrow \quad \mathrm{d}\tilde{x} = R\,\mathrm{d}R, \tag{3.13}$$

(3.10) is then written as

$$\frac{\mathrm{d}}{\mathrm{d}\tilde{x}}\left(\int_{Z_P}^{Z_S} U_0\,\mathrm{d}Z\right) + \frac{1}{2\tilde{x}}\int_{Z_P}^{Z_S} (U_0 + V_0)\,\mathrm{d}Z - \alpha = 0. \tag{3.14}$$

Note that the integrated continuity result shown in (3.14), expressed in terms of the mass flux through the lubrication gap, is solely due to the kinematic boundary condition at the solid surfaces and is not altered by the slip of the gas at the surfaces.

Recall that we decompose the velocities U_0 and V_0 into a sum of Poiseuille, Couette and plug flows, denoted by superscripts p, c, g respectively, yielding

$$\left.\begin{aligned} U_0 &= U_0^p + U_0^c + U_0^g, \\ V_0 &= V_0^p + V_0^c + V_0^g. \end{aligned}\right\} \tag{3.15}$$

The pressure field is related to the flux through the gap. To leading order, the pressure is uniform across the gap (i.e. $\partial P_0/\partial Z = 0$). Generalizing (3.3) to the two-dimensional flow within the gap, the relations for the integral of velocities U_0^p and V_0^p are (Cercignani &

https://doi.org/10.1017/jfm.2021.308 Published online by Cambridge University Press

Daneri 1963)

$$\int_{Z_P}^{Z_S} U_0^p \,\mathrm{d}Z = -\frac{1}{2}\frac{\delta^2}{\delta_0^3} g(\delta) \frac{\partial P_0}{\partial R}, \tag{3.16}$$

$$\int_{Z_P}^{Z_S} V_0^p \,\mathrm{d}Z = \frac{1}{2}\frac{\delta^2}{\delta_0^3} g(\delta) \frac{P_0}{R}. \tag{3.17}$$

Couette flow does not contribute to the flux

$$\int_{Z_P}^{Z_S} U_0^c \,\mathrm{d}Z = \int_{Z_P}^{Z_S} V_0^c \,\mathrm{d}Z = 0, \tag{3.18}$$

and for plug flow the integrals of the velocities are

$$\int_{Z_P}^{Z_S} U_0^g \,\mathrm{d}Z = -\int_{Z_P}^{Z_S} V_0^g \,\mathrm{d}Z = \tfrac{1}{2}(1-\omega). \tag{3.19}$$

Substituting these expressions into (3.14) yields a differential equation for the non-continuum pressure. To simplify the result, we introduce the notation

$$\tilde{q} = \frac{P_0}{R}. \tag{3.20}$$

Notice that only the integrals of the velocities due to Poiseuille flow contain the pressure, while (3.19) can be combined with the 'α' in (3.14) to give $(2\alpha - 1 + \omega)$. Factoring that quantity out of (3.14) yields the following

$$2\tilde{x}\delta^2 g q'' + \left[2\tilde{x}\frac{\mathrm{d}(\delta^2 g)}{\mathrm{d}\tilde{x}} + 4\delta^2 g\right] q' + \frac{\mathrm{d}(\delta^2 g)}{\mathrm{d}\tilde{x}} q = -\delta_0^3, \tag{3.21}$$

where

$$\left.\begin{aligned} q' \equiv \frac{\mathrm{d}q}{\mathrm{d}\tilde{x}} &= \frac{1}{R^2}\frac{\partial P_0}{\partial R} - \frac{P_0}{R^3}, \\ q'' \equiv \frac{\mathrm{d}^2 q}{\mathrm{d}\tilde{x}^2} &= \frac{1}{R^3}\frac{\partial^2 P_0}{\partial R^2} - \frac{3}{R^4}\frac{\partial P_0}{\partial R} + \frac{3P_0}{R^5}, \end{aligned}\right\} \tag{3.22}$$

and q is $\tilde{q}$ rescaled as follows to separate translational and rotational motions

$$\tilde{q} = q(2\alpha - 1 + \omega). \tag{3.23}$$

In the limit of pure translation, $\omega \to 0$ and therefore $\tilde{q} = q(2\alpha - 1)$. In the limit of pure rotation, $\omega \to \infty$, $\tilde{q} = q\omega$ and from (2.10) the pressure is rescaled as $p = \mu\Omega P \cos\theta$. Note that the definition of q precisely eliminates the singularity (at $r = 0$) in the differential equation. The numerical solution for q of interest is finite at $\tilde{x} = 0$ and asymptotes to the continuum pressure q_∞ as $\tilde{x} \to \infty$ (O'Neill & Majumdar 1970)

$$q_\infty = \tfrac{1}{5H^2}. \tag{3.24}$$

The ratio of the non-continuum pressure to the continuum pressure as a function of δ_0 is shown in figure 6.

https://doi.org/10.1017/jfm.2021.308 Published online by Cambridge University Press

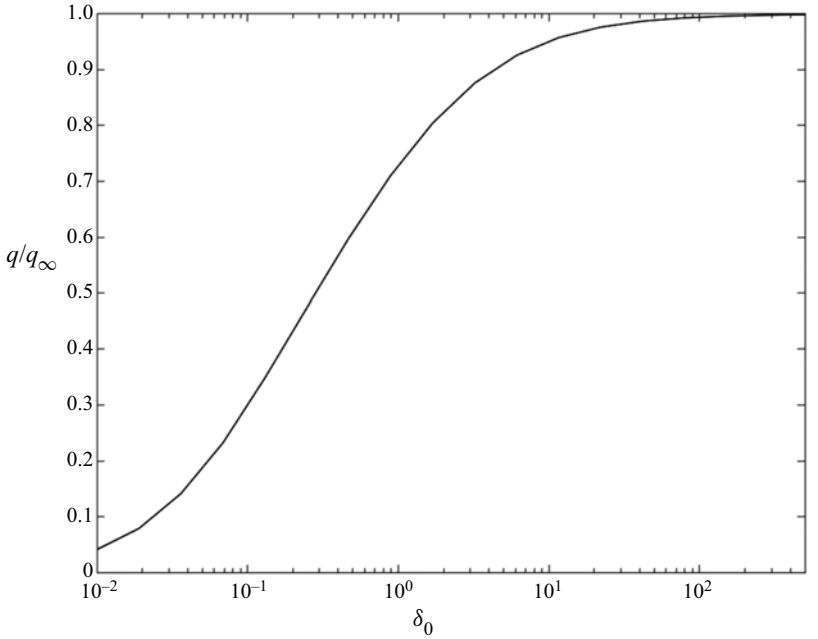


Figure 6. Graph of non-continuum pressure normalized by the continuum pressure on the axis between the centres plotted against rarefied parameter δ_0.

3.3. *Force and torque from inner region*

The force exerted by the fluid in the inner region of the surface of the particles is comprised of the force due to pressure (Poiseuille flow) and the force arising from the shear stresses (Poiseuille and Couette flows).

The force due to pressure is calculated by integrating minus the pressure times the unit outward normal on the surface, $\boldsymbol{n}_P$ and $\boldsymbol{n}_S$ for spheres P and S, respectively, over the sphere surface. The unit normals can be approximated as

$$\left.\begin{aligned} \boldsymbol{n}_P &= \boldsymbol{e}_z + \frac{r}{a_P}\sin\theta\ \boldsymbol{e}_y + \frac{r}{a_P}\cos\theta\ \boldsymbol{e}_x, \\ \boldsymbol{n}_S &= -\boldsymbol{e}_z + \frac{r}{a_S}\sin\theta\ \boldsymbol{e}_y + \frac{r}{a_S}\cos\theta\ \boldsymbol{e}_x, \end{aligned}\right\} \tag{3.25}$$

where $\boldsymbol{e}_x$, $\boldsymbol{e}_y$ and $\boldsymbol{e}_z$ are unit normals pointing in the x, y and z directions, respectively. Recall the pressure to leading order in ε can be expressed as

$$p(r,\theta,z) = \varepsilon^{-3/2}\frac{\mu U_S}{a}P_0(R)\cos\theta, \tag{3.26}$$

where $P_0(R)$ is determined by integrating (3.21) and using the relationships $P_0 = \tilde{q}\sqrt{2\tilde{x}}$ and $\tilde{x} = R^2/2$. We are interested in the contribution to the force acting in the x-direction (i.e. tangential), which is obtained by integrating minus the pressure times the x component of the unit normal over the surface of both spheres. Because the pressure acts normal to the sphere surfaces it produces no torque on the spheres. The result is

$$-\int_0^{r_M}\int_0^{2\pi} p\boldsymbol{n}_P\cdot\boldsymbol{e}_x\,\mathrm{d}\theta\ r\,\mathrm{d}r = -6\pi\mu U_S a(2\alpha-2)\int_0^{\tilde{x}_M}\tilde{x}\tilde{q}\,\mathrm{d}\tilde{x}. \tag{3.27}$$

https://doi.org/10.1017/jfm.2021.308 Published online by Cambridge University Press

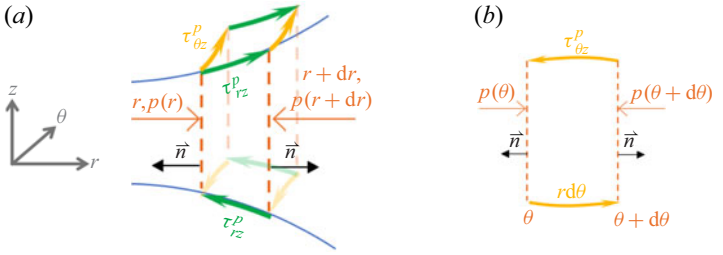


Figure 7. Momentum balance in the rz plane (a) and in the θz plane (b) due to Poiseuille flow only in the local gap in cylindrical polar coordinates.

A momentum balance on the inner region is used to construct the components of the shear stress due to Poiseuille flow in the rz and θz planes, as shown in figure 7. The resulting expressions are

$$\tau^p_{rz} = \frac{1}{2}h(r)\frac{\partial p}{\partial r}, \tag{3.28}$$

$$\tau^p_{\theta z} = \frac{1}{2}\frac{h(r)}{r}\frac{\partial p}{\partial \theta}, \tag{3.29}$$

where the superscript 'p' indicates the shear stress due to Poiseuille flow and the subscripts are the coordinate directions. Resolving the stress acting in the x direction yields

$$\tau^p_{xz} = \tau^p_{rz}\cos\theta - \tau^p_{\theta z}\sin\theta. \tag{3.30}$$

Substituting (3.26) and integrating the result over the sphere surfaces allows us to calculate the force and torque due to the shear stress from Poiseuille flow.

Finally, we consider the shear stress due to Couette flow in the gap, which can be written as (cf. (3.5), (3.8) and (3.9))

$$\tau^c_{xz} = -\frac{\mu U_{wall}}{\sqrt{\pi}h_0}\delta_0\eta(\delta), \tag{3.31}$$

where the superscript 'c' indicates the shear stress due to Couette flow. Integrating this quantity over the surface of the two spheres enables the calculation of the force and torque due to the shear stress from Couette flow.

We obtain the total force acting on each sphere in the tangential (x) direction by summing the contribution from the pressure (Poiseuille flow) and shear stresses (Poiseuille and Couette flows). Likewise, we can compute the total torque by summing the contributions due to the Poiseuille and Couette stresses. The tangential force and torque acting on a sphere due to its translation and rotation are non-dimensionalized as follows

$$\hat{f}^{\perp}_{t,i} = \frac{F^{\perp}_{t,i}}{-6\pi\mu a U_S}, \quad \hat{f}^{\perp}_{r,i} = \frac{F^{\perp}_{r,i}}{-6\pi\mu a(a_S\Omega)}, \tag{3.32a,b}$$

$$\hat{t}^{\perp}_{t,i} = \frac{T^{\perp}_{t,i}}{-8\pi\mu a a_i U_S}, \quad \hat{t}^{\perp}_{r,i} = \frac{T^{\perp}_{r,i}}{-8\pi\mu a a_i(a_S\Omega)}, \tag{3.33a,b}$$

where the subscript i refers to sphere P or S and the hat above the variable indicates the contribution from the inner region.

Integrating the radial direction up to the non-dimensional radial distance R_M, which lies in the range $\delta_0^{-1/2} \ll R_M \ll \varepsilon^{-1/2}$, yields the following expressions for the dimensionless

https://doi.org/10.1017/jfm.2021.308 Published online by Cambridge University Press

non-continuum inner forces and torques

$$\left.\begin{aligned}
\hat{f}_{t,S}^{\perp NC} &= \frac{1}{3\sqrt{\pi}}\int_{\delta_0}^{\delta_M}\eta(\delta)\,\mathrm{d}\delta + (2\alpha-1)(\tilde{x}Hq)_M + (2\alpha-1)^2\int_0^{\tilde{x}_M}\tilde{x}q\,\mathrm{d}\tilde{x},\\
\hat{f}_{t,P}^{\perp NC} &= -\frac{1}{3\sqrt{\pi}}\int_{\delta_0}^{\delta_M}\eta(\delta)\,\mathrm{d}\delta + (2\alpha-1)(\tilde{x}Hq)_M - (2\alpha-1)^2\int_0^{\tilde{x}_M}\tilde{x}q\,\mathrm{d}\tilde{x},\\
\hat{f}_{r,S}^{\perp NC} &= -\frac{1}{3\sqrt{\pi}}\int_{\delta_0}^{\delta_M}\eta(\delta)\,\mathrm{d}\delta + (\tilde{x}Hq)_M + (2\alpha-1)\int_0^{\tilde{x}_M}\tilde{x}q\,\mathrm{d}\tilde{x},\\
\hat{f}_{r,P}^{\perp NC} &= \frac{1}{3\sqrt{\pi}}\int_{\delta_0}^{\delta_M}\eta(\delta)\,\mathrm{d}\delta + (\tilde{x}Hq)_M - (2\alpha-1)\int_0^{\tilde{x}_M}\tilde{x}q\,\mathrm{d}\tilde{x},
\end{aligned}\right\} \tag{3.34}$$

$$\left.\begin{aligned}
\hat{t}_{t,S}^{\perp NC} &= -\frac{1}{4\sqrt{\pi}}\int_{\delta_0}^{\delta_M}\eta(\delta)\,\mathrm{d}\delta - \frac{3}{4}(2\alpha-1)(\tilde{x}Hq)_M + \frac{3}{4}(2\alpha-1)\int_0^{\tilde{x}_M}\tilde{x}q\,\mathrm{d}\tilde{x},\\
\hat{t}_{t,P}^{\perp NC} &= -\frac{1}{4\sqrt{\pi}}\int_{\delta_0}^{\delta_M}\eta(\delta)\,\mathrm{d}\delta + \frac{3}{4}(2\alpha-1)(\tilde{x}Hq)_M - \frac{3}{4}(2\alpha-1)\int_0^{\tilde{x}_M}\tilde{x}q\,\mathrm{d}\tilde{x},\\
\hat{t}_{r,S}^{\perp NC} &= \frac{1}{4\sqrt{\pi}}\int_{\delta_0}^{\delta_M}\eta(\delta)\,\mathrm{d}\delta - \frac{3}{4}(\tilde{x}Hq)_M + \frac{3}{4}\int_0^{\tilde{x}_M}\tilde{x}q\,\mathrm{d}\tilde{x},\\
\hat{t}_{r,P}^{\perp NC} &= \frac{1}{4\sqrt{\pi}}\int_{\delta_0}^{\delta_M}\eta(\delta)\,\mathrm{d}\delta + \frac{3}{4}(\tilde{x}Hq)_M - \frac{3}{4}\int_0^{\tilde{x}_M}\tilde{x}q\,\mathrm{d}\tilde{x},
\end{aligned}\right\} \tag{3.35}$$

where $\tilde{x}_M = R_M^2/2$, $\delta_M \equiv \delta_0(1+\tilde{x}_M)$ and $(\tilde{x}Hq)_M \equiv \tilde{x}_M(1+\tilde{x}_M)q(\tilde{x}_M)$. The superscript '*NC*' is added to indicate the non-continuum inner solution. To complete the analysis, we supplement the inner contribution for the forces and torques with the outer contributions computed for continuum flow using a multipole solution to obtain an expression that is valid for all ε in § 3.5. However, we first demonstrate that the non-continuum inner expressions derived herein are consistent with the classical analysis for a continuum fluid with 'slip' boundary conditions in § 3.4.

3.4. *Relationship to classical slip analysis*

The earliest work to introduce the first effects of the discrete nature of the gas was carried out by Hocking (1973). For $\delta_0 \gg 1$, he modelled the flow using the continuum momentum equation, but replaced the no-slip boundary condition with the Maxwell slip boundary condition, as shown below for translational and rotational motions

$$\left.\begin{aligned}
U_0(R,Z_P) - \beta\left.\frac{\partial U_0}{\partial Z}\right|_{Z_P} &= V_0(R,Z_P) - \beta\left.\frac{\partial V_0}{\partial Z}\right|_{Z_P} = 0,\\
U_0(R,Z_S) + \beta\left.\frac{\partial U_0}{\partial Z}\right|_{Z_S} &= V_0(R,Z_S) + \beta\left.\frac{\partial V_0}{\partial Z}\right|_{Z_S} = 1-\omega,
\end{aligned}\right\} \tag{3.36}$$

where β is the slip coefficient defined as

$$\beta \equiv \frac{k_1}{\delta_0}, \tag{3.37}$$

and recall $k_1 = 1.016$ as predicted by the BGK theory (Loyalka & Ferziger 1967).

https://doi.org/10.1017/jfm.2021.308 Published online by Cambridge University Press

We now show that this earlier analysis is consistent with the present work. The differential equation for the non-continuum pressure is shown in (3.21). If we replace $g(\delta)$ by the form it takes in the slip regime, $g(\delta) = \delta/6 + k_1$, we obtain the following differential equation for the pressure, originally derived by Hocking (1973)

$$2\tilde{x}H^2(H+6\beta)q_S'' + H[2\tilde{x}(3H+12\beta) + 4H(H+6\beta)]q_S' + H(3H+12\beta)q_S = -1, \tag{3.38}$$

where q_S indicates the continuum pressure with slip boundary conditions, scaled similarly as $\tilde{q}$ in (3.23). Likewise, substituting $\eta_S(\delta) = \sqrt{\pi}/(\delta + 2k_1)$ into the expressions for the force and torque given in (3.34) and (3.35), the inner resistivities reduce to the form derived by Hocking (1973) (note that Hocking presented combined effects due to translational and rotational motions and defined the resistivity for torque with the opposite sign convention to this paper)

$$\left.\begin{aligned}
\hat{f}_{t,S}^{\perp S} &= \frac{1}{3}\ln\left(\frac{1+\tilde{x}_M+2\beta}{1+2\beta}\right) + (2\alpha-1)(\tilde{x}Hq_S)_M + (2\alpha-1)^2\int_0^{\tilde{x}_M}\tilde{x}q_S\,\mathrm{d}\tilde{x},\\
\hat{f}_{t,P}^{\perp S} &= -\frac{1}{3}\ln\left(\frac{1+\tilde{x}_M+2\beta}{1+2\beta}\right) + (2\alpha-1)(\tilde{x}Hq_S)_M - (2\alpha-1)^2\int_0^{\tilde{x}_M}\tilde{x}q_S\,\mathrm{d}\tilde{x},\\
\hat{f}_{r,S}^{\perp S} &= -\frac{1}{3}\ln\left(\frac{1+\tilde{x}_M+2\beta}{1+2\beta}\right) + (\tilde{x}Hq_S)_M + (2\alpha-1)\int_0^{\tilde{x}_M}\tilde{x}q_S\,\mathrm{d}\tilde{x},\\
\hat{f}_{r,P}^{\perp S} &= \frac{1}{3}\ln\left(\frac{1+\tilde{x}_M+2\beta}{1+2\beta}\right) + (\tilde{x}Hq_S)_M - (2\alpha-1)\int_0^{\tilde{x}_M}\tilde{x}q_S\,\mathrm{d}\tilde{x},
\end{aligned}\right\} \tag{3.39}$$

$$\left.\begin{aligned}
\hat{t}_{t,S}^{\perp S} &= -\frac{1}{4}\ln\left(\frac{1+\tilde{x}_M+2\beta}{1+2\beta}\right) - \frac{3}{4}(2\alpha-1)(\tilde{x}Hq_S)_M + \frac{3}{4}(2\alpha-1)\int_0^{\tilde{x}_M}\tilde{x}q_S\,\mathrm{d}\tilde{x},\\
\hat{t}_{t,P}^{\perp S} &= -\frac{1}{4}\ln\left(\frac{1+\tilde{x}_M+2\beta}{1+2\beta}\right) + \frac{3}{4}(2\alpha-1)(\tilde{x}Hq_S)_M - \frac{3}{4}(2\alpha-1)\int_0^{\tilde{x}_M}\tilde{x}q_S\,\mathrm{d}\tilde{x},\\
\hat{t}_{r,S}^{\perp S} &= \frac{1}{4}\ln\left(\frac{1+\tilde{x}_M+2\beta}{1+2\beta}\right) - \frac{3}{4}(\tilde{x}Hq_S)_M + \frac{3}{4}\int_0^{\tilde{x}_M}\tilde{x}q_S\,\mathrm{d}\tilde{x},\\
\hat{t}_{r,P}^{\perp S} &= \frac{1}{4}\ln\left(\frac{1+\tilde{x}_M+2\beta}{1+2\beta}\right) + \frac{3}{4}(\tilde{x}Hq_S)_M - \frac{3}{4}\int_0^{\tilde{x}_M}\tilde{x}q_S\,\mathrm{d}\tilde{x},
\end{aligned}\right\} \tag{3.40}$$

where the superscript 'S' designates the continuum equations with slip boundary conditions. The above expressions differ from Hocking (1973) in that the term $(\tilde{x}Hq_S)_M$ was approximated by $\tilde{x}_M^2 q_S(\tilde{x}_M)$; however, assuming $\tilde{x}_M \gg 1$, the difference is inconsequential.

The inner solution for the continuum equations with 'no-slip' boundary conditions are recovered by setting $k_1 = 0$ and therefore $\beta = 0$. The equation for the pressure reduces to

$$2\tilde{x}H^3 q_C'' + 2H^2(2H+3\tilde{x})q_C' + 3H^2 q = -1, \tag{3.41}$$

where q_C designates the continuum pressure with no-slip boundary conditions, scaled similarly as $\tilde{q}$ in (3.23). The result is consistent with the equation derived by O'Neill & Majumdar (1970) when written in terms of P_0 and R, and using their definition for

https://doi.org/10.1017/jfm.2021.308 Published online by Cambridge University Press

the size ratio. A particular solution for this differential equation is

$$q_C = \frac{1}{5H^2}. \tag{3.42}$$

Setting $k_1 = \beta = 0$ and introducing (3.42) into (3.39) and (3.40) yields the inner contribution to the resistivity functions for the continuum equations with no-slip boundary conditions

$$\left.\begin{aligned}
\hat{f}^{\perp C}_{t,S} &= \left[\tfrac{1}{3} + \tfrac{1}{5}(2\alpha-1)^2\right]\ln(1+\tilde{x}_M) + \tfrac{2}{5}(1-\alpha)(2\alpha-1),\\
\hat{f}^{\perp C}_{t,P} &= \left[-\tfrac{1}{3} - \tfrac{1}{5}(2\alpha-1)^2\right]\ln(1+\tilde{x}_M) + \tfrac{2}{5}\alpha(2\alpha-1),\\
\hat{f}^{\perp C}_{r,S} &= \left[-\tfrac{1}{3} + \tfrac{1}{5}(2\alpha-1)\right]\ln(1+\tilde{x}_M) + \tfrac{2}{5}(1-\alpha),\\
\hat{f}^{\perp C}_{r,P} &= \left[\tfrac{1}{3} - \tfrac{1}{5}(2\alpha-1)\right]\ln(1+\tilde{x}_M) + \tfrac{2}{5}\alpha,
\end{aligned}\right\} \tag{3.43}$$

$$\left.\begin{aligned}
\hat{t}^{\perp C}_{t,S} &= \left[-\tfrac{1}{4} + \tfrac{3}{20}(2\alpha-1)\right]\ln(1+\tilde{x}_M) - \tfrac{3}{10}(2\alpha-1),\\
\hat{t}^{\perp C}_{t,P} &= \left[-\tfrac{1}{4} - \tfrac{3}{20}(2\alpha-1)\right]\ln(1+\tilde{x}_M) - \tfrac{3}{10}(2\alpha-1),\\
\hat{t}^{\perp C}_{r,S} &= \tfrac{2}{5}\ln(1+\tilde{x}_M) - \tfrac{3}{10},\\
\hat{t}^{\perp C}_{r,P} &= \tfrac{1}{10}\ln(1+\tilde{x}_M) + \tfrac{3}{10}.
\end{aligned}\right\} \tag{3.44}$$

The superscript 'C' indicates these are solutions to the continuum equations with no-slip boundary conditions. O'Neill & Stewartson (1967) derived results for the pure translation of a sphere parallel to a plane, which corresponds to setting $\alpha = 1$ yielding $\hat{f}^{\perp C}_{t,S} = 8(\ln(1+\tilde{x}_M))/15$. Consistent with Jeffrey & Onishi (1984) and O'Neill & Stewartson (1967), the $O(1)$ term vanishes for $\alpha = 1$.

3.5. *Uniformly valid solution*

As discussed by O'Neill & Stewartson (1967), for a lubrication flow, the inner region corresponds to the domain where the pressure and velocity gradients are large and the lubrication approximation is valid. The inner solution will transition from the free molecular regime ($\delta_0 \ll 1$) to the continuum regime ($\delta_0 \gg 1$) depending upon the value of δ_0. As we are restricting this investigation to the limit $Kn \ll 1$ (recall the particle Knudsen number is defined as $Kn \equiv \lambda/a$), the outer flow, which scales with the sphere radius, will always be in the continuum regime, regardless of the regime of the inner flow. Hence the outer region is governed by the Stokes equation (2.2*a*,*b*). Complete solutions for the forces and torques are obtained by summing the contributions from the inner and outer regions.

To simplify the nomenclature, we will temporarily drop references to a particular resistivity, and define $\hat{f}$ as the 'inner' contribution to a given resistivity and $\check{f}$ as the continuum 'outer' contribution to the same resistivity. The inner and outer solutions for a continuum fluid take the form

$$\left.\begin{aligned}
\hat{f}^C &= \hat{A}^C(\alpha) + B(\alpha)\ln\left(\frac{r_M}{h_0}\right),\\
\check{f} &= \check{A}(\alpha) + B(\alpha)\ln\left(\frac{a}{r_M}\right),
\end{aligned}\right\} \tag{3.45}$$

https://doi.org/10.1017/jfm.2021.308 Published online by Cambridge University Press

where the superscript 'C' denotes the continuum inner solution, r_M is the boundary between the inner and outer regions and $\hat{A}^C(\alpha)$, $\check{A}(\alpha)$ and $B(\alpha)$ are coefficients that depend on the size ratio, α. Note that the functional form for the inner solution in (3.45) is taken from Jeffrey & Onishi (1984) for no-slip boundary conditions in the limit $\tilde{x}_M \gg 1$. The matched asymptotic solution for the continuum model of lubrication flow then takes the form (Jeffrey & Onishi 1984; O'Neill & Majumdar 1970)

$$f^C = \hat{f}^C + \check{f} = \hat{A}^C(\alpha) + \check{A}(\alpha) + B(\alpha)\ln\left(\frac{1}{\varepsilon}\right). \tag{3.46}$$

Notice that the dependence on r_M cancels out of the expression, so long as it lies within $(ah_0)^{1/2} \ll r_M \ll a$, where the approximations in (3.45) are valid.

Equations (3.34) and (3.35) have the following asymptotic form

$$\hat{f}^{NC} = \hat{A}^{NC}(\alpha, \delta_0) + B(\alpha)\ln\left(\frac{r_M}{h_0}\right). \tag{3.47}$$

The matched asymptotic expression for the uniformly valid resistivity for lubrication flow is then given by

$$f^{UV} = \hat{f}^{NC} + \check{f} = \hat{A}^{NC}(\alpha, \delta_0) + \check{A}(\alpha) + B(\alpha)\ln\left(\frac{1}{\varepsilon}\right), \tag{3.48}$$

where the superscript 'UV' refers to the uniformly valid lubrication flow solution corresponding to $\varepsilon \ll 1$ and $\delta_0 = O(1)$. Alternatively, the uniformly valid resistivity could be constructed as follows

$$f^{UV} = f^C + \Delta f, \tag{3.49}$$

where

$$\Delta f \equiv \hat{f}^{NC} - \hat{f}^C. \tag{3.50}$$

Then, Δf is found by subtracting the inner lubrication solutions for a continuum, (3.43) and (3.44), from (3.34) and (3.35). For example, evaluating $\Delta f^{\perp}_{t,S} \equiv \hat{f}^{\perp \mathrm{NC}}_{t,S} - \hat{f}^{\perp C}_{t,S}$ yields

$$\begin{aligned}\Delta f^{\perp}_{t,S} = {} & \frac{1}{3\sqrt{\pi}}\int_{\delta_0}^{\delta_M} \Delta\eta(\delta)\,\mathrm{d}\delta + (2\alpha-1)^2\int_0^{\tilde{x}_M}\tilde{x}\Delta q\,\mathrm{d}\tilde{x} \\ & + \frac{1}{3\sqrt{\pi}}\int_{\delta_0}^{\delta_M}\eta_C(\delta)\,\mathrm{d}\delta + (2\alpha-1)(\tilde{x}Hq)_M + (2\alpha-1)^2\int_0^{\tilde{x}_M}\tilde{x}q_C\,\mathrm{d}\tilde{x} - \hat{f}^{\perp C}_{t,S},\end{aligned} \tag{3.51}$$

where $\Delta\eta(\delta) \equiv \eta(\delta) - \eta_C(\delta)$ and $\Delta q \equiv q - q_C$. In light of the analysis presented in § 3.4, the expression on the second line of (3.51) can be shown to vanish, yielding

$$\Delta f^{\perp}_{t,S} = \frac{1}{3\sqrt{\pi}}\int_{\delta_0}^{\delta_M}\Delta\eta(\delta)\,\mathrm{d}\delta + (2\alpha-1)^2\int_0^{\tilde{x}_M}\tilde{x}\Delta q\,\mathrm{d}\tilde{x}. \tag{3.52}$$

It is convenient to define the integrals as

$$\tilde{W}(\delta_0) \equiv \int_{\delta_0}^{\delta_M}\Delta\eta(\delta)\,\mathrm{d}\delta, \tag{3.53}$$

$$\tilde{Q}(\delta_0) \equiv \int_0^{\tilde{x}_M}\tilde{x}\Delta q\,\mathrm{d}\tilde{x}. \tag{3.54}$$

https://doi.org/10.1017/jfm.2021.308 Published online by Cambridge University Press

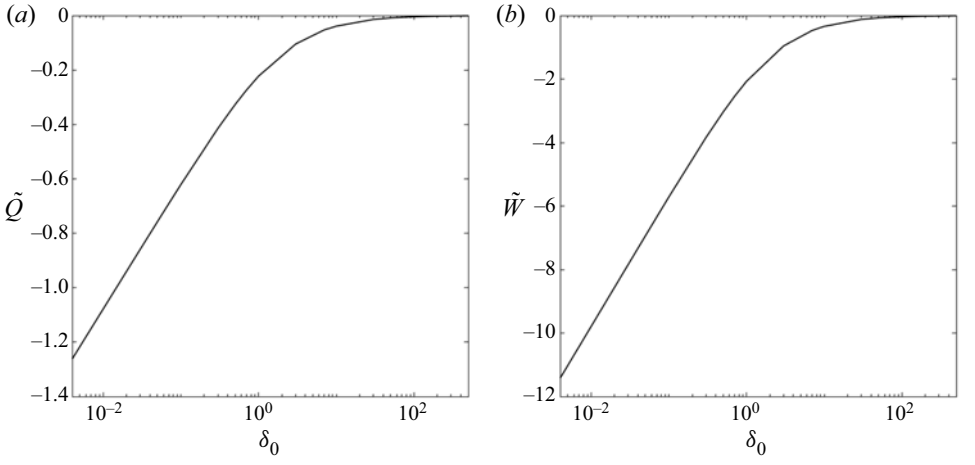


Figure 8. Graph of generalized pressure force function $\tilde{Q}$ (*a*) and stress function $\tilde{W}$ (*b*) as functions of δ_0 to describe the tangential resistivities for any size ratio and at any gap separation.

Figure 8 shows the behaviour of $\tilde{W}(\delta_0)$ and $\tilde{Q}(\delta_0)$ as a function of δ_0. This behaviour can be well approximated by the following fitted functions

$$\tilde{Q} = \frac{b_1 + b_2 \ln\left(\dfrac{1}{\delta_0} + b_3\right)}{1 + b_4\delta_0}, \tag{3.55}$$

where $b_1 = -0.1580$, $b_2 = -1/5$, $b_3 = 0.65632$, $b_4 = 0.16330$ and

$$\tilde{W} = \frac{b_5 + b_6 \ln\left(\dfrac{1}{\delta_0} + b_7\right)}{1 + b_8\delta_0}, \tag{3.56}$$

where $b_5 = -1.6448$, $b_6 = -\sqrt{\pi}$, $b_7 = 0.59098$, $b_8 = 0.19167$. The relative error is less than 2 % over the entire range.

Applying this procedure to all the expressions in (3.34) and (3.35) yields

$$\left.\begin{aligned} \Delta f^{\perp}_{t,S} = -\Delta f^{\perp}_{t,P} = \tfrac{1}{3\sqrt{\pi}}\tilde{W} + (2\alpha-1)^2\tilde{Q}, \\ \Delta f^{\perp}_{r,S} = -\Delta f^{\perp}_{r,P} = -\tfrac{1}{3\sqrt{\pi}}\tilde{W} + (2\alpha-1)\tilde{Q}, \end{aligned}\right\} \tag{3.57}$$

$$\left.\begin{aligned} \Delta t^{\perp}_{t,S} = -\tfrac{1}{4\sqrt{\pi}}\tilde{W} + \tfrac{3}{4}(2\alpha-1)\tilde{Q}, \\ \Delta t^{\perp}_{t,P} = -\tfrac{1}{4\sqrt{\pi}}\tilde{W} - \tfrac{3}{4}(2\alpha-1)\tilde{Q}, \\ \Delta t^{\perp}_{r,S} = \tfrac{1}{4\sqrt{\pi}}\tilde{W} + \tfrac{3}{4}\tilde{Q}, \\ \Delta t^{\perp}_{r,P} = \tfrac{1}{4\sqrt{\pi}}\tilde{W} - \tfrac{3}{4}\tilde{Q}. \end{aligned}\right\} \tag{3.58}$$

Figure 9 shows $\Delta f^{\perp}_{t,S}$ as a function of δ_0. Notice that the function approaches zero for large δ_0 since the non-continuum inner solution approaches the continuum inner solution in that limit. Jeffrey & Onishi (1984) derived generalized expressions, and developed FORTRAN codes, for the continuum resistivities that smoothly transition from twin

https://doi.org/10.1017/jfm.2021.308 Published online by Cambridge University Press

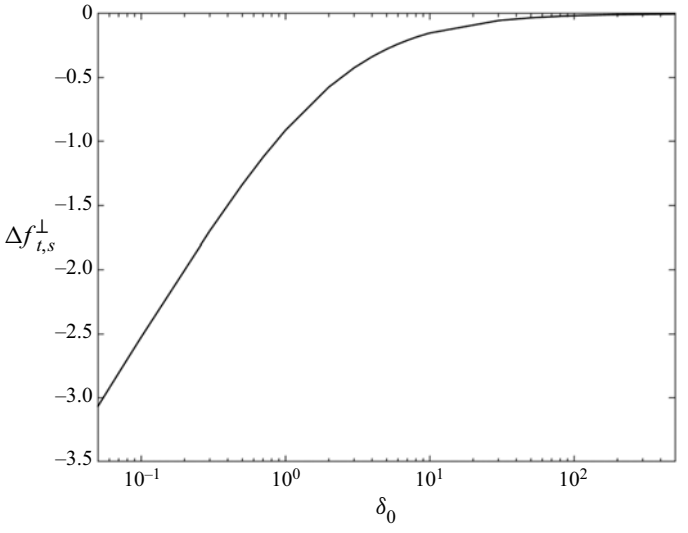


Figure 9. Example of $\Delta f_t^{\perp} = \hat{f}_t^{NC} - \hat{f}_t^{C}$ obtained from (3.50) for $\alpha = 1$. Non-continuum effects, corresponding to $\Delta f_t^{\perp} < 0$, are readily apparent for small δ_0, whereas the function approaches zero in the continuum limit, corresponding to $\delta_0 \gg 1$.

multipole expansions at large separations (O'Neill & Majumdar 1970) to the matched asymptotic solutions in the lubrication regime shown in (3.46). These expressions can be extended to incorporate non-continuum lubrication flows, for $Kn \ll 1$, yielding uniformly valid resistivity functions, valid for arbitrary ε, as follows

$$\left.\begin{aligned}
f_{t,S}^{\perp UV} &= f_{t,S}^{\perp JO}(\varepsilon,\alpha) + \Delta f_{t,S}^{\perp}(\delta_0,\alpha),\\
f_{t,P}^{\perp UV} &= f_{t,P}^{\perp JO}(\varepsilon,\alpha) + \Delta f_{t,P}^{\perp}(\delta_0,\alpha),\\
f_{r,S}^{\perp UV} &= f_{r,S}^{\perp JO}(\varepsilon,\alpha) + \Delta f_{r,S}^{\perp}(\delta_0,\alpha),\\
f_{r,P}^{\perp UV} &= f_{r,P}^{\perp JO}(\varepsilon,\alpha) + \Delta f_{r,P}^{\perp}(\delta_0,\alpha),\\
t_{t,S}^{\perp UV} &= t_{t,S}^{\perp JO}(\varepsilon,\alpha) + \Delta t_{t,S}^{\perp}(\delta_0,\alpha),\\
t_{t,P}^{\perp UV} &= t_{t,P}^{\perp JO}(\varepsilon,\alpha) + \Delta t_{t,P}^{\perp}(\delta_0,\alpha),\\
t_{r,S}^{\perp UV} &= t_{r,S}^{\perp JO}(\varepsilon,\alpha) + \Delta t_{r,S}^{\perp}(\delta_0,\alpha),\\
t_{r,P}^{\perp UV} &= t_{r,P}^{\perp JO}(\varepsilon,\alpha) + \Delta t_{r,P}^{\perp}(\delta_0,\alpha),
\end{aligned}\right\} \tag{3.59}$$

where the superscript '*JO*' refers to the generalized resistivity functions taken from Jeffrey & Onishi (1984). Further details on the three-dimensional formulation of these equations are provided in Appendix A.

Figure 10 shows $f_{t,S}^{\perp}$, $t_{t,S}^{\perp}$ and $t_{r,S}^{\perp}$ computed in various ways vs ε at the indicated Knudsen numbers. In the large ε limit, all three solutions approach the continuum solution, f_t^C (solid line). The open circles were computed from (3.59) using (3.57), (3.58) and the curve fits for $\tilde{Q}$ and $\tilde{W}$ given in (3.55) and (3.56). The dotted green line shows the non-continuum lubrication approximation (3.49), which is valid in the limit of small ε where the overall resistivity is dominated by the non-continuum inner resistivity. In this limit, each resistivity can be shown analytically to approach a constant. In the limit as $\delta_0 \to 0$, (3.55) and (3.56)

https://doi.org/10.1017/jfm.2021.308 Published online by Cambridge University Press

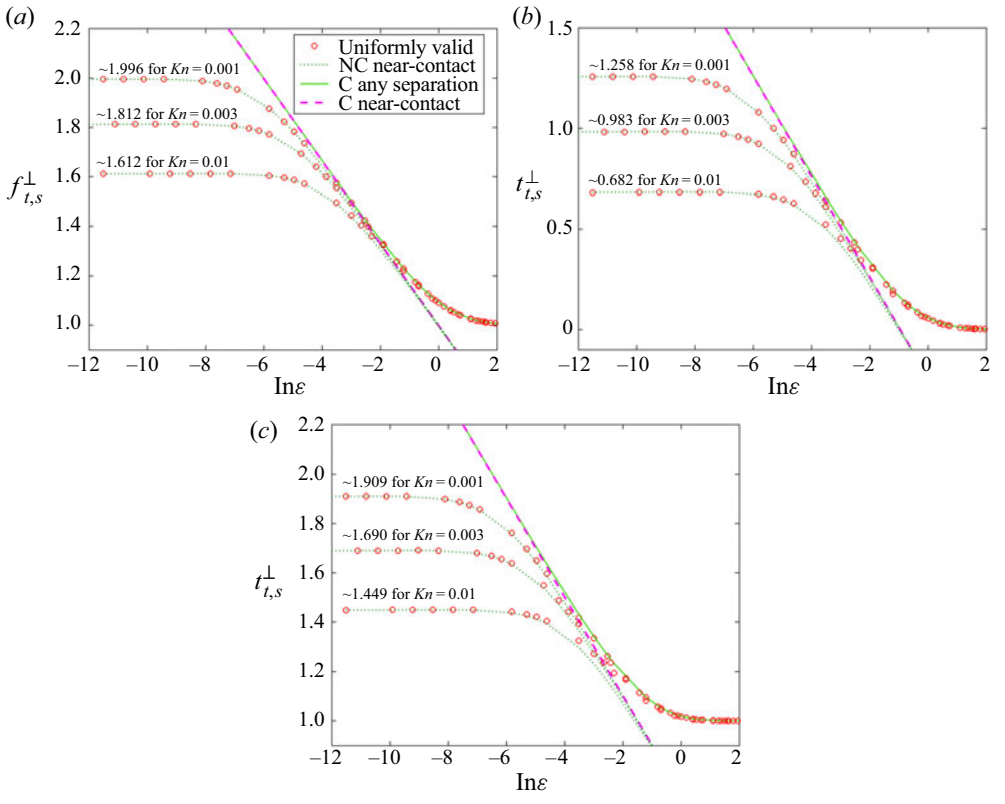


Figure 10. The force on sphere S due to translation (a), $f^{\perp}_{t,S}$, torque due to translation (b), $t^{\perp}_{t,S}$, and torque due to rotation (c), $t^{\perp}_{r,S}$, is plotted as a function of ε for Knudsen numbers 0.01, 0.003 and 0.001 and $\alpha = 0.5$. The open circles use (3.59), the dotted green line uses (3.49), the solid green line shows the generalized expression from Jeffrey & Onishi (1984) and the magenta dashed line is using (3.46).

reduce to

$$\left.\begin{aligned} \tilde{Q} &\to b_1 + b_2 \ln\left(\frac{1}{\delta_0}\right), \\ \tilde{W} &\to b_5 + b_6 \ln\left(\frac{1}{\delta_0}\right), \end{aligned}\right\} \tag{3.60}$$

which when substituted into (3.59) yields the asymptote as a function of Kn

$$\left.\begin{aligned} f^{\perp UV}_{t,S} &\to \left[-\frac{4}{15}\alpha(3\alpha^2 - 3\alpha + 2)\right]\ln(Kn) + \alpha\left[b_1(2\alpha-1)^2 + \frac{b_5}{3\sqrt{\pi}}\right] + A^{Y}_{22}(\alpha), \\ t^{\perp UV}_{t,S} &\to \left[\frac{1}{5}\alpha(3\alpha - 4)\right]\ln(Kn) - 2\alpha\left[\frac{3}{4}b_1(2\alpha-1) - \frac{b_5}{4\sqrt{\pi}}\right] + B^{Y}_{22}(\alpha), \\ t^{\perp UV}_{r,S} &\to \left[-\frac{2}{5}\alpha\right]\ln(Kn) + \alpha\left[\frac{3}{4}b_1 + \frac{b_5}{4\sqrt{\pi}}\right] + C^{Y}_{22}(\alpha), \end{aligned}\right\} \tag{3.61}$$

where $A^{Y}_{22}(0.5) = 0.9983$, $B^{Y}_{22}(0.5) = -0.2390$ and $C^{Y}_{22}(0.5) = 0.7028$ are the values for the $O(1)$ terms, respectively, for $\alpha = 0.5$ (Jeffrey & Onishi 1984). There are only a few

https://doi.org/10.1017/jfm.2021.308 Published online by Cambridge University Press

tabulated values provided in Jeffrey & Onishi (1984) so we modified their FORTRAN code to output the $O(1)$ terms for any size ratio. Figure 10 shows the asymptotic values of the resistivities in the limit as $\varepsilon \to 0$ for the different Knudsen numbers that were calculated.

It is well known that the tangential force due to particle rotation and the torque due to tangential relative translation satisfy the reciprocal relation

$$\frac{f_{r,S}^{\perp JO}}{t_{t,S}^{\perp JO}} = \frac{4}{3}. \tag{3.62}$$

This equation was derived by Lorentz (1896) using the reciprocal theorem for the continuum Stokes flow equations and a no-slip boundary condition. However, a derivation based on Onsager's reciprocal relations (Onsager 1931*a*,*b*) for near equilibrium fluids can be used to show that the same relation holds for particles in any fluid exhibiting a linear response due to a small deviation from equilibrium (Landau & Lifshitz 1980; Ying & Peters 1989; Zhang, Xu & Qian 2015) including a non-continuum gas governed by the linearized Boltzmann equation and a gas described using the Stokes equations with a Maxwell slip boundary condition. Consistent with this expectation, we can see from (3.57) and (3.58) that

$$\frac{\Delta f_{r,S}^{\perp}}{\Delta t_{t,S}^{\perp}} = \frac{4}{3}, \tag{3.63}$$

implying

$$\frac{f_{r,S}^{\perp UV}}{t_{t,S}^{\perp UV}} = \frac{4}{3} \tag{3.64}$$

at all separations.

4. Sphere settling adjacent to a vertical wall

The canonical problem of a sphere settling adjacent to a vertical wall in an otherwise quiescent, semi-infinite fluid is considered by setting $\alpha = 1$. At steady state, the sphere is assumed to have a translational velocity U_S and a rotation rate $a_S\Omega$, as illustrated in figure 11. The steady state results from a force and torque balance. Introducing the resistance functions derived earlier we have

$$F_H \equiv -6\pi\mu a(U_S f_{t,S}^{\perp UV} + a_S\Omega f_{r,S}^{\perp UV}), \tag{4.1}$$

such that the resulting force balance in the x-direction is

$$F_x = F_g + F_H = 0, \tag{4.2}$$

where $F_g = mg$ is the force due to gravity. In the absence of external torques, the resultant torque acting on the particle in the y-direction is

$$T_y = -8\pi\mu a a_S \left(U_S t_{t,S}^{\perp UV} + a_S\Omega t_{r,S}^{\perp UV}\right) = 0. \tag{4.3}$$

Notice that only the tangential resistivities are involved in this motion. From equations (4.1) and (4.3), the force balance becomes

$$6\pi\mu a U_S \left[f_{t,S}^{\perp UV} + \omega f_{r,S}^{\perp UV}\right] = mg, \tag{4.4}$$

https://doi.org/10.1017/jfm.2021.308 Published online by Cambridge University Press

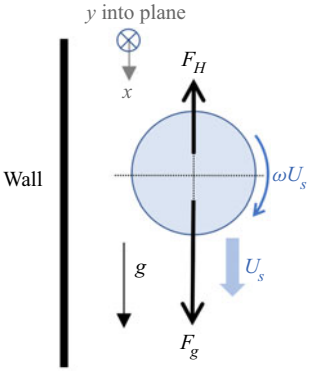


Figure 11. Sketch of a particle settling vertically with a wall at steady state where hydrodynamic F_H forces are balanced by gravitational force F_g.

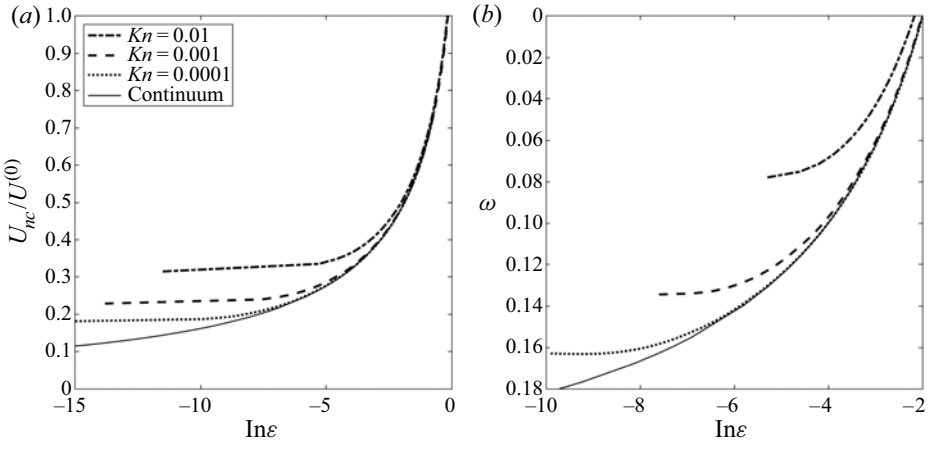


Figure 12. Graph of non-continuum settling velocity normalized by the settling velocity of the isolated particle (a) and ratio of angular to translational velocities ω (b) at different ε for spheres with Knudsen numbers of 0.01, 0.001 and 0.0001.

where ω is determined by

$$\omega = -\frac{t_{t,S}^{\perp UV}}{t_{r,S}^{\perp UV}}. \tag{4.5}$$

We analyse the motion of spheres with Knudsen numbers 0.01, 0.001 and 0.0001. We solve (4.5) for ω and substitute that into (4.4) to obtain U_S. Figure 12(a) shows the normalized settling velocity $U_S/U^{(0)}$, where $U^{(0)}$ is the terminal velocity in an unbounded fluid and $\varepsilon = h_0/a$, and (b) shows the rotation rate ω as a function of ε.

Goldman, Cox & Brenner (1967) analysed a sphere in a continuum fluid settling under gravity adjacent to a vertical plane and argued that a no-slip condition would require $\omega = 1$, and since their continuum results indicated an asymptotic value of 0.25 in the limit as $\varepsilon \to 0$, the sphere has to roll and slip. Our non-continuum results show even lower asymptotic values of ω, suggesting even greater slipping is occurring than for the continuum case. To our knowledge, no experimental measurements exist in this regime.

https://doi.org/10.1017/jfm.2021.308 Published online by Cambridge University Press

A second observation pertains to the discrepancy between the continuum and non-continuum settling velocities in the limit as the gap goes to zero. The continuum approximation predicts the velocity vanishes in this limit, or equivalently the sphere will 'stick' to the wall due to the diverging hydrodynamic force. Figure 12(*a*) shows that the non-continuum theory predicts a constant settling velocity as the gap goes to zero. The experiment by Carty (1957) yielded a terminal speed for a sphere near a wall that was constant for small gap separations, consistent with the prediction of the non-continuum theory; however, Goldman *et al.* (1967) noted their results were also consistent with solid-body friction caused by surface roughness, underscoring the need for experiments in which the effects due to roughness have been carefully eliminated.

5. Conclusions

In this paper, we have derived uniformly valid resistivity functions for the forces and torques between two unequal size spheres moving or rotating through a gas in a direction perpendicular to their line of centres at low Reynolds and Mach numbers. The expressions were derived using a matched asymptotic analysis taking into consideration the non-continuum flow that occurs between the spheres when their minimum separation distance is comparable to or smaller than the mean free path of the gas. The analysis assumes the Knudsen number is small such that the non-continuum flow is restricted to the inner lubrication region. The lubrication flow was expressed as a superposition of its three constituent flows: Poiseuille flow, Couette flow and plug flow. The relative weights of the three flows were determined by the boundary conditions and by the pressure field. To account for the non-continuum flow in the gap, we applied the solutions for Poiseuille flow and Couette flow found by Cercignani & Pagani (1966), who solved the BGK approximation to the linearized Boltzmann equation. Substituting these expressions into the lubrication approximation for the flow in the gap yielded the differential equation describing the pressure and the stress that then could be integrated over the surface of the sphere to obtain the non-continuum 'inner' solution for the force and torque acting on the sphere. As we are interested in spheres with asymptotically small Knudsen numbers, the outer flow is always in the continuum regime regardless of the gap separation. A non-continuum correction to the inner solution was obtained by subtracting the inner solution for the continuum fluid from the inner solution for the non-continuum fluid and curve fitting the result. Adding to that the generalized resistivity functions for a continuum fluid derived by Jeffrey & Onishi (1984) yielded uniformly valid expressions for the four tangential resistivity functions that smoothly transition from the continuum expressions for $\delta_0 \gg 1$ to the free molecular expressions for $\delta_0 \ll 1$.

For spheres nearly in contact, the continuum tangential resistivities diverge logarithmically with decreasing gap separation. However, in the pseudo-free molecular regime, the non-continuum lubrication flow yields resistivities that asymptote to a constant that scales like $\ln(Kn^{-1})$. We apply the resulting expressions to the case of a sphere settling adjacent to a vertical wall. At separations large in comparison to the mean free path of the gas, the sphere settles and rotates at rates that correspond to the continuum solution. As the minimum gap separation approaches and goes below the mean free path of the gas, the settling speed and rotation rate are modified by the non-continuum flow; the settling speed is increased and the dimensionless rotation rate, $a_S\Omega/U_S$, is decreased, but $a_S\Omega$ is increased relative to the continuum fluid. For a sphere in contact with the wall, the continuum solution predicts the velocity and rotation of the sphere vanish causing the sphere to 'stick' to the wall due to hydrodynamic resistance only, whereas the

https://doi.org/10.1017/jfm.2021.308 Published online by Cambridge University Press

non-continuum resistivities yield a finite settling and rotation speed at contact, consistent with experiments (Carty 1957).

A primary motivation for this study is to resolve the near-contact motion of cloud droplets in the atmosphere. The continuum lubrication flow generates a normal force that diverges like ε^{-1} and a tangential force that diverges like $\ln(\varepsilon^{-1})$. As a consequence, two cloud droplets on a colliding trajectory would not be able to come into physical contact, as the resistive force would stop their relative motion. This would imply that cloud droplets could only grow by condensation. The results developed here, along with the earlier work of Sundararajakumar & Koch (1996), provide a complete explanation for coalescence in the Stokes regime, namely the weaker lubrication forces that result from the non-continuum lubrication flow between the droplets at gap separations below the mean free path of the gas allow coalescence to occur in finite time. Thus, the resistance functions developed in this paper play a critical role in understanding the evolution of atmospheric clouds.

Acknowledgements. This study was supported by the National Science Foundation grant number CBET 1605195. The authors gratefully acknowledge the National Center for Atmospheric Research (NCAR) for providing high performance computing resources on Cheyenne.

Declaration of interests. The authors report no conflict of interest.

Author ORCIDs.
Melanie Li Sing How https://orcid.org/0000-0002-5416-8584;
Donald L. Koch https://orcid.org/0000-0002-5474-879X;
Lance R. Collins https://orcid.org/0000-0002-1792-9479.

Appendix A. Vector formulation of the non-continuum resistivity tensor

This appendix presents the vector formulation for the resistivity tensor for two particles moving through a quiescent fluid. We begin with the continuum formulation of Jeffrey & Onishi (1984), and incorporate the uniformly valid tangential expressions developed herein and the uniformly valid expressions derived by Sundararajakumar & Koch (1996) for the normal force. It should be noted that the scaling used by Jeffrey & Onishi (1984) to non-dimensionalize the equations differs from ours. They used the arithmetic mean radius for their length scale and introduced a size ratio, κ, defined as

$$\kappa = \frac{a_2}{a_1}, \tag{A1}$$

which is related to α by

$$\alpha = \frac{1}{1+\kappa}. \tag{A2}$$

Throughout the appendix, we have adapted the expressions derived in this paper to their basis to simplify the evaluation of the uniformly valid expressions. Furthermore, we replace the labels 'P' and 'S' with '1' and '2' to facilitate writing the tensor relationships. The analysis in the appendix allows both spheres to move – the motion of each sphere induces a force and torque on each sphere, giving rise to four separate interactions. We introduce the subscripts '$\gamma\sigma$' to represent the force (or torque) acting on sphere γ due to the motion of sphere σ, where γ and σ can each be either 1 or 2. We extend the expressions derived in the paper to the general case.

https://doi.org/10.1017/jfm.2021.308 Published online by Cambridge University Press

The equation for the force and torque acting on particles 1 and 2 can be written as (Jeffrey & Onishi 1984)

$$\begin{pmatrix} \boldsymbol{F}_1 \\ \boldsymbol{F}_2 \\ \boldsymbol{T}_1 \\ \boldsymbol{T}_2 \end{pmatrix} = \begin{pmatrix} \boldsymbol{A}_{11} & \boldsymbol{A}_{12} & \tilde{\boldsymbol{B}}_{11} & \tilde{\boldsymbol{B}}_{12} \\ \boldsymbol{A}_{21} & \boldsymbol{A}_{22} & \tilde{\boldsymbol{B}}_{21} & \tilde{\boldsymbol{B}}_{22} \\ \boldsymbol{B}_{11} & \boldsymbol{B}_{12} & \boldsymbol{C}_{11} & \boldsymbol{C}_{12} \\ \boldsymbol{B}_{21} & \boldsymbol{B}_{22} & \boldsymbol{C}_{21} & \boldsymbol{C}_{22} \end{pmatrix} \begin{pmatrix} \boldsymbol{U}_1 \\ \boldsymbol{U}_2 \\ \boldsymbol{\Omega}_1 \\ \boldsymbol{\Omega}_2 \end{pmatrix} \tag{A3}$$

where $\boldsymbol{F}_1, \boldsymbol{F}_2, \boldsymbol{T}_1$ and $\boldsymbol{T}_2$ are the forces and torques acting on particles 1 and 2, $\boldsymbol{A}$, $\boldsymbol{B}$, $\tilde{\boldsymbol{B}}$ and $\boldsymbol{C}$ are second rank tensors (defined below) and $\boldsymbol{U}_1$, $\boldsymbol{U}_2$, $\boldsymbol{\Omega}_1$ and $\boldsymbol{\Omega}_2$ are the translational and rotational velocities for particles 1 and 2. We define the separation vector, $\boldsymbol{r} \equiv \boldsymbol{x}_2 - \boldsymbol{x}_1$, where $\boldsymbol{x}_1$ and $\boldsymbol{x}_2$ are the positions of the centres of particles 1 and 2, respectively. The unit vector along the line of centres is $\hat{\boldsymbol{r}} \equiv \boldsymbol{r}/|\boldsymbol{r}|$. The minimum gap separation between the particles is then $h_0 = |\boldsymbol{r}| - (a_1 + a_2)$, and we retain the definitions of ε and δ_0 from the main paper.

It is convenient to introduce index notation such that $A_{ij}^{\gamma\sigma} = \boldsymbol{A}_{\gamma\sigma}$, where indices i and j indicate directions and γ and σ are either 1 or 2. For example, $\boldsymbol{A}_{12} = A_{ij}^{12}$. The tensors in (A3) are then given in dimensional form consistent with the notations of Jeffrey & Onishi (1984) (note the difference with the (3.32*a*,*b*) and (3.33*a*,*b*) in the main paper)

$$A_{ij}^{\gamma\sigma} = -6\pi\mu \left(\frac{a_\gamma + a_\sigma}{2}\right) [f_{t,\gamma\sigma}^{\parallel UV} \hat{r}_i \hat{r}_j + f_{t,\gamma\sigma}^{\perp UV} (\delta_{ij} - \hat{r}_i \hat{r}_j)], \tag{A4}$$

$$B_{ij}^{\gamma\sigma} = -4\pi\mu \left(\frac{a_\gamma + a_\sigma}{2}\right)^2 t_{t,\gamma\sigma}^{\perp UV} \epsilon_{ijk} \hat{r}_k, \tag{A5}$$

$$\tilde{B}_{ij}^{\gamma\sigma} = -4\pi\mu \left(\frac{a_\gamma + a_\sigma}{2}\right)^2 t_{t,\sigma\gamma}^{\perp UV} \epsilon_{jik} \hat{r}_k, \tag{A6}$$

$$C_{ij}^{\gamma\sigma} = -8\pi\mu \left(\frac{a_\gamma + a_\sigma}{2}\right)^3 [t_{r,\gamma\sigma}^{\parallel JO} \hat{r}_i \hat{r}_j + t_{r,\gamma\sigma}^{\perp UV} (\delta_{ij} - \hat{r}_i \hat{r}_j)], \tag{A7}$$

where $\hat{r}_i$ is the unit normal vector pointing from particle 1 to particle 2, δ_{ij} is the Kronecker delta function and ϵ_{ijk} is the alternating unit tensor. The scalar resistivity functions are defined as

$$f_{t,\gamma\sigma}^{\perp UV} = Y_{\gamma\sigma}^{A}(\varepsilon, \kappa) + (-1)^{(\gamma+\sigma)} a_{\gamma\sigma} \left[\frac{1}{3\sqrt{\pi}} \tilde{W}(\delta_0) + \left(\frac{1-\kappa}{1+\kappa}\right)^2 \tilde{Q}(\delta_0)\right], \tag{A8}$$

$$t_{t,\gamma\sigma}^{\perp UV} = Y_{\gamma\sigma}^{B}(\varepsilon, \kappa) + 2a_{\gamma\sigma} \left(\frac{a_\gamma}{a_m}\right)^{|\gamma-\sigma|} \left[\frac{(-1)^\sigma}{4\sqrt{\pi}} \tilde{W}(\delta_0) - (-1)^{(\gamma+\sigma)} \frac{3}{4} \left(\frac{1-\kappa}{1+\kappa}\right) \tilde{Q}(\delta_0)\right], \tag{A9}$$

$$t_{r,\gamma\sigma}^{\perp UV} = Y_{\gamma\sigma}^{C}(\varepsilon, \kappa) + a_{\gamma\sigma} \left(\frac{2a}{a_m}\right)^{|\gamma-\sigma|} \left[\frac{1}{4\sqrt{\pi}} \tilde{W}(\delta_0) + (-1)^{(\gamma+\sigma)} \frac{3}{4} \tilde{Q}(\delta_0)\right], \tag{A10}$$

where $a_m \equiv (a_1 + a_2)/2$ is the arithmetic mean radius,

$$a_{\gamma\sigma} \equiv a \left(\frac{a_\gamma + a_\sigma}{2}\right)^{-1}, \tag{A11}$$

and $Y_{\gamma\sigma}^{A}$, $Y_{\gamma\sigma}^{B}$ and $Y_{\gamma\sigma}^{C}$ are the tangential resistivities defined in Jeffrey & Onishi (1984).

https://doi.org/10.1017/jfm.2021.308 Published online by Cambridge University Press

The normal resistivity, $f_{t,\gamma\sigma}^{\parallel UV}$ is given by

$$f_{t,\gamma\sigma}^{\parallel UV} = X_{\gamma\sigma}^{A}(\epsilon,\kappa) + (-1)^{(\gamma+\sigma)} a_{\gamma\sigma}\left(\frac{f_{fit}^{\parallel}(\delta_0,\kappa)}{Kn} - \frac{1}{\varepsilon}\right), \tag{A12}$$

where $X_{\gamma\sigma}^{A}$ is the continuum resistivity (Jeffrey & Onishi 1984) and $f_{fit}^{\parallel}$ can be expressed as (Sundararajakumar & Koch 1996)

$$f_{fit}^{\parallel} = \begin{cases} \dfrac{\pi}{6}\left(\ln t - \dfrac{1}{t} - \dfrac{1}{t^2} - \dfrac{2}{t^3}\right) & \\ \quad +1.5475\delta_0^2 + 0.7896\delta_0 + 0.4094 & (\delta_0 < 0.35) \\ 0.00006\left(\dfrac{1}{\delta_0}\right)^3 - 0.00172\left(\dfrac{1}{\delta_0}\right)^2 + 0.0169\left(\dfrac{1}{\delta_0}\right) & \\ \quad 0.1769\ln\left(\dfrac{1}{\delta_0}\right) + 0.3744 & (0.35 < \delta_0 < 0.9) \\ 0.00050\delta_0^4 - 0.00835\delta_0^3 + 0.05605\delta_0^2 - 0.2196\delta_0 + 0.5661 & \\ \quad -0.0055\left(\dfrac{1}{\delta_0}\right) - 0.01965\left(\dfrac{1}{\delta_0}\right)^2 + 0.0231\left(\dfrac{1}{\delta_0}\right)^3 & (0.9 < \delta_0 < 4.4) \\ \dfrac{1}{18k_1^2}\left[(6k_1+\delta_0)\ln\left(1+\dfrac{6k_1}{\delta_0}\right) - 6k_1\right] & (\delta_0 > 4.4) \end{cases} \tag{A13}$$

and $t = \ln(1/\delta_0) + 0.8$. We note that the coefficients in (A13) differ from those in Sundararajakumar & Koch (1996) because we did not apply the correction factor $\sqrt{\pi}/2$ to the mean free path from the BGK theory to make it consistent with that for a hard sphere gas, as they did. While that correction factor can be easily incorporated into the normal resistivity, for which the pressure equation can be integrated analytically, the same correction applied to the tangential resistivities introduces a discontinuity into the equation for the pressure field that precludes its numerical integration. Consequently, we use the BGK mean free path throughout for consistency. Finally, we note that there is no non-continuum flow generated by the torque acting in the normal direction, $t_{r,\gamma\sigma}^{\parallel JO} \equiv X_{\gamma\sigma}^{C}$, and hence we apply the Jeffrey & Onishi (1984) expression directly.

We make available an open source code that computes the above equations.

References

Batchelor, G.K. 1982 Sedimentation in a dilute polydisperse system of interacting spheres. Part I. General theory. *J. Fluid Mech.* **119**, 379–408.

Bhatnagar, P.L., Gross, E.P. & Krook, M. 1954 A model for collision processes in gases. I. Small amplitude processes in charged and neutral one-component systems. *Phys. Rev.* **94** (3), 511–525.

Brenner, H. & O'Neill, M.E. 1972 On the Stokes resistance of a multiparticle systems in a linear shear field. *Chem. Engng Sci.* **27**, 1421–1439.

Carty, J.J. 1957 Resistance coefficients for spheres on a plane boundary. Master's thesis, MIT.

Cercignani, C. & Daneri, A. 1963 Flow of a rarefied gas between two parallel plates. *J. Appl. Phys.* **34**, 3509–3513.

Cercignani, C. & Pagani, C.D. 1966 Variational approach to boundary-value problems in kinetic theory. *Phys. Fluids* **9**, 1167–1173.

Davis, R.H., Schonberg, J.A. & Rallison, J.M. 1989 The lubrication force between two viscous drops. *Phys. Fluids* A **1**, 77–81.

Devenish, B.J., *et al.* 2012 Droplet growth in warm turbulent clouds. *Q. J. R. Meteorol. Soc.* **138**, 1401–1429.

https://doi.org/10.1017/jfm.2021.308 Published online by Cambridge University Press

DHANASEKARAN, J., ROY, A. & KOCH, D.L. 2021 Collision rate of bidisperse spheres settling in a compressional non-continuum gas flow. *J. Fluid Mech.* **910**, A10.

GOLDMAN, A.J., COX, R.G. & BRENNER, H. 1967 Slow viscous motion of a sphere parallel to a plane wall – I: motion through a quiescent fluid. *Chem. Engng Sci.* **22**, 637–651.

GOPINATH, A., CHEN, S.B. & KOCH, D.L. 1997 Lubrication flows between spherical particles colliding in a compressible non-continuum gas. *J. Fluid Mech.* **344**, 245–269.

HAPPEL, J. & BRENNER, H. 1983 *Low Reynolds Number Hydrodynamics with Special Applications to Particulate Media*. Springer.

HOCKING, L.M. 1973 The effect of slip on the motion of a sphere close to a wall and of two adjacent spheres. *J. Engng Maths* **7**, 207–221.

HOCKING, L.M. & JONAS, P.R. 1970 The collision efficiency of small drops. *Q. J. R. Meteorol. Soc.* **96**, 722–729.

JEFFREY, D.J. & ONISHI, Y. 1984 Calculation of the resistance and mobility functions for two unequal rigid spheres in low-Reynolds-number flow. *J. Fluid Mech.* **139**, 261–290.

KIM, S. & KARRILA, S.J. 1991 *Microhydrodynamics: Principles and Selected Applications*. Butterworth-Heinemann.

KLINZING, G.E. 2001 Pneumatic conveying: transport solutions, pitfalls, and measurements. In *Handbook of Powder Technology* (ed. A. Levy & H. Kalman), pp. 291–301. Elsevier.

KOGAN, M.N. 1969 *Rarefied Gas Dynamics*. Plenum.

LANDAU, L.D. & LIFSHITZ, E.M. 1980 *Statistical Physics*. Butterworth-Heinemann.

LORENTZ, H.A. 1896 A general theorem concerning the motion of a viscous fluid and a few consequences derived from it. *Z. Koninkl. Akad. van Wetensch. Amsterdam* **5**, 168–175.

LOYALKA, S.K. & FERZIGER, J.H. 1967 Model dependence of the slip coefficient. *Phys. Fluids* **10**, 1833–1839.

O'NEILL, M.E. & MAJUMDAR, S.R. 1970 Asymmetrical slow viscous fluid motions caused by the translation or rotation of two spheres. Part II: asymptotic forms of the solutions when the minimum clearance between the spheres approaches zero. *Z. Angew. Math. Phys.* **21**, 180–187.

O'NEILL, M.E. & STEWARTSON, K. 1967 On the slow motion of a sphere parallel to a nearby plane wall. *J. Fluid Mech.* **27**, 705–724.

ONSAGER, L. 1931*a* Reciprocal relations in irreversible processes. I. *Phys. Rev.* **37**, 405–426.

ONSAGER, L. 1931*b* Reciprocal relations in irreversible processes. II. *Phys. Rev.* **38**, 2265–2279.

SHARIPOV, F. 2016 Analytical and numerical calculations of rarefied gas flows. In *Handbook of Vacuum Technology* (ed. K. Jousten), pp. 167–228. Wiley-vch.

SHAW, R.A. 2003 Particle-turbulence interactions in atmospheric clouds. *Annu. Rev. Fluid Mech.* **35**, 183–227.

SUNDARARAJAKUMAR, R.R. & KOCH, D.L. 1996 Non-continuum lubrication flows between particles colliding in a gas. *J. Fluid Mech.* **313**, 238–308.

YING, R. & PETERS, M.H. 1989 Hydrodynamic interaction of two unequal-sized spheres in a slightly rarefied gas: resistance and mobility functions. *J. Fluid Mech.* **207**, 353–378.

ZHANG, J., XU, X. & QIAN, T. 2015 Anisotropic particle in viscous shear flow: Navier slip, reciprocal symmetry, and Jeffery orbit. *Phys. Rev.* E **91**, 033016.

https://doi.org/10.1017/jfm.2021.308 Published online by Cambridge University Press